Hu et al. *Zool. Res. Divers. Conserv.* 2025, 2(1): 14−31
https://doi.org/10.24272/j.issn.2097-3772.2024.019
https://cstr.cn/32249.14.zrdc.2024.019

ZRDC Zoological Research: Diversity and Conservation

Article Open Access

Revisiting the taxonomy and distribution of *Miniopterus* (Chiroptera: Miniopteridae) bats in China based upon an integrated molecular-ecological-morphological approach

Yi-Feng Hu[1,2,#], Xiao-Yun Wang[2,#], Yi Wu[2], Masaharu Motokawa[3,*], Wen-Hua Yu[2,*]

[1] *Graduate School of Science*, *Kyoto University*, *Sakyo*, *Kyoto* 606-8502, *Japan*

[2] *Key Laboratory of Conservation and Application in Biodiversity of South China*, *School of Life Sciences*, *Guangzhou University*, *Guangzhou*, *Guangdong* 510006, *China*

[3] *Kyoto University Museum*, *Kyoto University*, *Sakyo*, *Kyoto* 606-8501, *Japan*

ABSTRACT

Three common species of *Miniopterus fuliginosus*, *M. magnater* and *M. pusillus* are known to inhabit China. However, *M. fuliginosus* and *M. magnater* are so similar in external morphology as to pose great challenges for accurate classification. Furthermore, taxonomic statuses, distribution ranges and taxonomic keys of these three species have remained controversial. For addressing these outstanding issues, the authors integrated molecular phylogenetic analyses, ensemble species distribution models (ESDMs), multiple morphological comparisons and decision tree algorithms for reassessing their taxonomy and distribution in China. Mitochondrial cytochrome c oxidase subunit I (*COI*) gene phylogeny revealed three distinct monophyletic groups corresponding to *M. fuliginosus*, *M. magnater* and *M. pusillus*. And the observed distribution patterns indicated *M. fuliginosus* had a broad distribution across China while *M. magnater* and *M. pusillus* exhibited a more restricted distribution, overlapping with *M. fuliginosus* in South China. And cranial morphometry indicated *M. magnater* was slightly larger than *M. fuliginosus* and significantly larger than *M. pusillus*. Also three-dimensional (3D) skull geomorphometry uncovered distinct features for each species in rostrum, braincase, tympanic bullae and mandibular shape. Decision tree algorithms helped to identify forearm length, braincase breadth and width across the third upper molars as three major taxonomic keys for assisting species identification. This study corroborated the importance of integrative approaches for identifying *Miniopterus* species and validated a methodological approach applicable to other cryptic species complexes.

Keywords: 3D geomorphometry; China; Decision tree algorithm; Ensemble species distribution model; *Miniopterus* species; Taxonomy

INTRODUCTION

Currently encompassing 42 recognized species within monotypic genus *Miniopterus*, the family Miniopteridae (Mammalia: Chiroptera) are widely distributed across tropical and subtropical regions of Old World (Goodman et al., 2015; Ibáñez & Juste, 2019; Kusuminda et al., 2022; Monadjem et al., 2019, 2020; Srinivasulu & Srinivasulu, 2023). However, taxonomy within this enigmatic taxon has remained controversial. Previously deemed with a virtual global distribution (Sanborn, 1931; Simmons, 2005), *M. schreibersii* is currently recognized as a diverse complex of several cryptic species, including *M. schreibersii*, *M. pallidus*, *M. fuliginosus*, *M. magnater*, *M. oceanensis* and *M. macrodens* (Appleton et al., 2004; Furman et al., 2009, 2010; Maeda, 1982; Tian et al., 2004).

Within China, Maeda (1982) and Tian et al. (2004) proposed that *M. schreibersii* sensu lato should be recognized as two distinct species of *M. fuliginosus* and *M. magnater* in light of skull variations across geographic populations and mitochondrial DNA-based genetic divergence. Furthermore, Li et al. (2015) noticed morphological differences, particularly in condylobasal length and width across the third upper molars not fully aligning with the taxonomic keys of Smith & Xie (2008). Based upon these findings, Li et al. (2015) advocated

Received: 22 November 2024; Accepted: 05 December 2024; Online: 06 December 2024

Foundation items: This work was supported by the National Natural Sciences Foundation of China (32192421), the Special Grant Foundations for National Science and & Technology Basic Research Program of China (2021FY100303), and the DFGP Project of Fauna of Guangdong Province (202115)

[#]Authors contributed equally to this work

*Corresponding authors, E-mail: motokawa.masaharu.6m@kyoto-u.ac.jp; wenhua_yu@gzhu.edu.cn

for species determination through molecular phylogenetics. Their study also mapped the geographic distributions of *M. fuliginosus* in North China, including Shaanxi, Henan, Anhui, Zhejiang, Jiangxi, Fujian, Hunan, Yunnan and Sichuan while *M. magnater* was restricted to South China in Hainan Island and Guangdong. Early studies suggested that *M. fuliginosus* extended farther south into Guangxi, Guangdong, Hong Kong, Hainan Island and Fujian, overlapping with *M. magnater* in Guangdong and Hainan Island (Maeda, 1982; Smith & Xie, 2008; Wang, 2003). These discrepant distribution patterns could be attributed to limited sampling of Li et al. (2015) or misidentifications in earlier records. Moreover, smaller-sized and cryptic species *M. pusillus*, also endemic in South China (Smith & Xie, 2008), has been long overlooked, further complicating the taxonomy and distribution of *Miniopterus* bats. These challenges affected not only taxonomists but also researchers of bat-related viruses and parasites, where accurate species identification remained critical.

For addressing the ongoing taxonomic and distributional challenges within *Miniopterus* genus in China, species distribution models (SDMs) might be employed as predictive tools through integrating species occurrences and environmental variables (Guisan & Thuiller, 2005). And SDMs have been widely applied for other bat groups (Bosso et al., 2018; Delgado-Jaramillo et al., 2020; Ke et al., 2024; Wieringa et al., 2021). In recent years, ensemble species distribution model (ESDM) approach, integrating multiple models into a consensus forecast, has gained a growing popularity for greater prediction accuracy and reliability (Araújo & New, 2007; Friedman & Popescu, 2008; Grenouillet et al., 2011; Hao et al., 2020; Hardy et al., 2011; Măntoiu et al., 2022; Oeser et al., 2024; Srinivasulu et al., 2024). For *Miniopterus*, this novel ESDM approach could improve the accuracy of their geographical range and help to identify potential niche differentiation and habitat preferences between closely related species (Novella-Fernandez et al., 2021; Smeraldo et al., 2021).

In parallel, skull geomorphometry has emerged as a powerful tool for unraveling complex morphological differences, particularly in species with high morphological similarity (Alhajeri, 2021; Marcus et al., 2013; Paluh & Bauer, 2017; Zelditch et al., 2012). Unlike traditional linear measurements, geomorphometry could separate size and shape components, allowing the detection of subtler cranial variations (Arbour et al., 2019). This approach enhanced statistical rigor and provided a visually descriptive portrayal of shape differences, complementing conventional linear measurements (Marcus et al., 2013; Zelditch et al., 2012). This approach has also introduced a new dimension to craniodental variation studies, enhancing the precision of taxonomic and evolutionary analyses.

Additionally, machine learning has revolutionized classification and prediction tasks across various disciplines (Das, 2015; Gao et al., 2018; Maniruzzaman et al., 2020; Sen et al., 2020). Decision tree algorithms are particularly well-suited for tackling classification and regression changes due to their interpretability, flexibility and robust statistical performance (Cao et al., 2020; Messner et al., 2020; Wan et al., 2020). These algorithms provide an efficient method for deliberate selection of key features and integration with other models, such as neural networks, enhancing their performance in complex scenarios (Brown et al., 1993; De'ath & Fabricius, 2000). Applying decision trees for *Miniopterus* classification is well-poised to boost the accuracy and reproducibility of species identification, providing taxonomists with a solution for distinguishing between cryptic and morphologically similar species.

Here we endeavor to 1) clarify the taxonomic status of three *Miniopterus* species through comprehensive statistical analyses of traditional morphometrics, landmark-based three-dimensional (3D) skull geometric morphometrics and molecular evidence; 2) predict and map the current distribution of *Miniopterus* species across China through an ESDM approach; 3) infer taxonomic keys for three *Miniopterus* species by using decision tree algorithms. By integrating these methodologies, this research attempted to provide a comprehensive understanding of taxonomy, species distribution, genetic differentiation and morphological variation of *Miniopterus* species in China.

MATERIALS AND METHODS

Sampling

Between 2000 and 2021, a total of 201 specimens of *Miniopterus* bats were collected across China, including Anhui (AH, *n*=3), Guangdong (GD, *n*=75), Guangxi (GX, *n*=8), Guizhou (GZ, *n*=10), Hainan Island (HNI, *n*=35), Hong Kong (HK, *n*=14), Hunan (HN, *n*=8), Hubei (HB, *n*=8), Jiangxi (JX, *n*=7), Yunnan (YN, *n*=22) and Zhejiang (ZJ, *n*=12). Species identification was initially determined from morphological size per the scheme of Smith & Xie (2008), with 58 specimens classified as *M. pusillus* based upon their significantly smaller external size. And the remaining 143 specimens were designated under the "*M. schreibersii*" species complex. This classification was subsequently confirmed through molecular phylogenetic analysis of mitochondrial cytochrome c oxidase subunit I (*COI*). All samples were deposited at School of Life Sciences of Guangzhou University (Guangzhou, China).

DNA extraction, sequencing and phylogenetic inference

Genomic DNA was extracted from muscle, liver or patagium tissue samples with a SteadyPure Universal Genomic DNA extraction Kit AG21009 (Accurate Biology, China). PCR amplification of a partial segment of *COI* gene was conducted in a 25 μL reaction with Accurate Taq PCR Kit AG1101 (Accurate Biology, China) via customized primers (HYF_forward: 5'-TCTGCTATTTGGTGCCTGAG-3'; HYF_reverse: 5'-AGAAGGTAGTGTTTAGGTTTCGA-3'). A total of 126 samples were successfully amplified and sequenced (Sangon, China) with sequences deposited in CNCB database (China National Center for Bioinformation) (refer to Supplementary Table S1 for accession numbers). Sequences were assembled and edited in SeqMan and EdiSeq (DNASTAR, Lasergene v.7.1) and subsequently combined with additional *Miniopterus COI* sequences from the NCBI-nt database (Supplementary Table S1). Alignment was performed through ClustalW (Thompson et al., 1994) with R package *msa* (Bodenhofer et al., 2015) in R software v.4.3.0 (The R Foundation, 2023). A maximum likelihood (ML) phylogenetic tree was constructed with TIM2+I+F+G4 model in IQ-TREE v.1.6.12 (Hoang et al., 2018; Nguyen et al., 2015). *Chaerephon plicatus* (*COI* sequences, HM540190, KP975244, MK817188) was designated as outgroup. The pseudo-replicate trees were generated with 1000 bootstrapping replicates for assessing branch supports. For further validating the topology and node support, a Bayesian phylogenetic tree

was constructed with GTR+G4 model in MrBayes v.3.2.7 (Ronquist et al., 2012). Bayesian analysis incorporated two independent runs of four Markov chain Monte Carlo (MCMC) chains, each running for 5 000 000 generations with sampling every 1 000 generations and diagnostics every 5 000 generations. Uncorrected genetic distances within and between species were calculated with MEGA v.11 (Tamura et al., 2021).

Ensemble species distribution modeling and forecasting

For elucidating the present distribution pattern of three *Miniopterus* species in China, QGIS software (v.3.34.1) was utilized for spatial mapping of their distribution areas. Occurrence data from China were compiled through integrating the sources of Global Biodiversity Information Facility (GBIF), relevant literature and location information for *Miniopterus* sequences available on the NCBI-nt database, as detailed in Supplementary Table S2 (Francis et al., 2010; Li et al., 2015; Liang et al., 2017; Smith & Xie, 2008; Wang, 2003; Wu et al., 2020; Zhang et al., 2018). For addressing collinearity between environmental variables and ensuring more parsimonious and interpretable models (Merow et al., 2013), vifstep function of R package *usdm* was selected (Naimi et al., 2014). Variables were selected for each of three *Miniopterus* species based upon analysis of variance inflation factor (VIF). A total of 11 bioclimatic variables (bio2, mean diurnal range; bio4, temperature seasonality; bio7, temperature annual range; bio8, mean temperature of wettest quarter; bio9, mean temperature of driest quarter; bio12, annual precipitation; bio13, precipitation of wettest month; bio14, precipitation of driest month; bio15, precipitation seasonality; bio18, precipitation of warmest quarter; bio19, precipitation of coldest quarter) and elevation (elev) were employed for current potential distribution pattern. All above-mentioned variables were derived from WorldClim (v.2.1) with 2.5 arc-minutes resolution (Fick & Hijmans, 2017). Environmental variables corresponding to the occurrence points were extracted with *raster* package in R (Hijmans et al., 2015) in preparation for subsequent species distribution modeling.

For assessing the current potential distributions of three *Miniopterus* species in China, eight modeling algorithms were employed in an ensemble model (Scherrer et al., 2019; Smeraldo et al., 2018) using R package *SSDM* (Schmitt et al., 2017). The algorithms selected for ensemble approach included generalized linear model (GLM), generalized additive model (GAM), multivariate adaptive regression splines (MARS), generalized boosted regressions model (GBM), classification tree analysis (CTA), random forest (RF), artificial neural network (ANN) and support vector machines (SVM). For accounting for observed long-distance migratory capability of *Miniopterus* species, resampling grid coefficient for occurrence points was set to “2” (Hutterer et al., 2005; Kimprasit et al., 2021; Rodrigues & Palmeirim, 2008; Xu et al., 2005). The ensemble selection criteria included an area under the curve (AUC) threshold of ≥0.75 (evaluating the model’s capability of distinguishing presences from absences), a Cohen’s Kappa threshold of ≥0.5 (for agreement between observed and predicted values), sensitivity and specificity thresholds of ≥0.75 (ensuring accurate identification of presences and absences) and a correct proportion (prop.correct) threshold of ≥0.75 (for overall prediction accuracy). Threshold precision was set at 101 for ensuring accuracy in model evaluation. And model evaluation was conducted with a holdout validation method, in which 70% of the data were reserved for training the models and 30% for evaluation. This process was systematically replicated 10 times. The accuracy of ESDM was assessed by the metrics of AUC, omission rate, sensitivity, specificity, proportion of correctly predicted occurrences (prop.correct) and Kappa scores. And response curve analysis was performed with R package *sdm* (Naimi & Araújo, 2016) for elucidating the relationship between environmental variables and species distributions.

Morphological measurements

For assessing the possible morphological differentiation among *M. fuliginosus*, *M. magnater* and *M. pusillus*, 6 external and 17 craniodental measurements were taken from 161 samples with a digital caliper (the nearest 0.1/0.01 mm). External measurements included head–body length (HBL), tail length (TL), ear length (EL), hindfoot length (HFL), forearm length (FAL) and tibia length (TibL) while craniodental measurements included greatest length of skull (GLS), occipital–canine length (OCL), condylobasal length (CBL), palate length (PL), zygomatic breadth (ZB), braincase breadth (BB), braincase height (BCH), mastoid width (MW), interorbital width (IOW), length of palate bridge (LPB), rostrum width across upper canines (C^1C^1), width across third upper molars (M^3M^3), upper canine–third molar length (C^1M^3), lower canine–third molar length (C_1M_3), width across third lower molars (M_3M_3), mandibular length (ML) and height of articular process of mandible (HCPM) (Supplementary Figure S1).

Various statistical analyses were employed for assessing the differences among three species, including analysis of variance (ANOVA) for comparisons among all three species, analysis of covariance (ANCOVA) with the greatest length of skull as a covariate for skull morphometry and principal component analysis (PCA) for skull morphometry. Sexual size dimorphism (SSD) for *M. fuliginosus* and *M. magnater* was evaluated with skull linear measurements through multivariate analysis of variance (MANOVA) and ANOVA. Due to a limited number of female samples, SSD analysis was skipped for *M. pusillus*. And geographical variation among three species within China was examined with MANOVA, followed by ANOVA. All statistical analyses were performed with R software.

Geomorphometry

For evaluating the geomorphometric shape variations in skulls of *M. fuliginosus*, *M. magnater* and *M. pusillus*, a Solutionix Rexcan DS3 Silver 3D Scanner (Solutionix, South Korea) is optimized for small objects. With a maximum resolution of 0.01 mm, this scanner was utilized for digitalizing 3D skull models. The outputs were subsequently saved as PHY files in ezScan 2017 software. A total of 68 crania and 84 mandibles were scanned. And landmarks and semi landmarks (patches) were placed with a 3D Slicer v.5.2.2 (Fedorov et al., 2012), an open-source software for visualization and analysis. Placement of these landmarks and patches was facilitated by built-in Markups function. Detailed descriptions of these points were provided in Supplementary Figure S2.

For extracting shape changes, Generalized Procrustes analysis (GPA) was performed. It referred to a process involving rescaling, translation and rotation of specimens to a common shape space (Rohlf & Slice, 1990). Procrustes-aligned specimens were projected onto tangent space with R

package *geomorph* (Adams et al., 2022). This process yielded a 3D array of Procrustes shape coordinates and a vector of centroid sizes. Centroid sizes were log-transformed (log (Size)) and employed as metrics of cranium and mandible sizes. For facilitating subsequent analyses, Procrustes shape coordinates were converted into a two-dimensional matrix with two.d.arry function from *geomorph* package, serving as proxies of shape variables. ANOVA was performed with procD.lm function from *geomorph* with ordinary least squares for model fitting. Significance testing was based upon 999 iterations of residual randomization. Type-I sums of squares and cross-product computations were applied for multifactorial models with the interaction factor defined as the greatest length of skull (GLS).

For visualizing shape differences, *SlicerMorph* extension package in 3D Slicer (Porto et al., 2021) was utilized for performing a PCA on Procrustes shape variables and identifying the main axes of shape variation. The first two PCs were visualized as scatterplots with interactive 3D skull models corresponding to the extremes of each PC axis. Then canonical variates analysis (CVA) was performed for elucidating group differences and predicting group segregation. CVA function from *Morpho* package (Schlager, 2017) was enabled with 3D skull models of two CV extremes and visualized with points3d function in *rgl* package (Adler & Murdoch, 2020). For examining the relationship between shape and size, common allometric component analysis (CAC) was performed with GLS as a metric for skull size. This analysis enabled plotAllometry function from *geomorph* package and CAC function from *Morpho* package. Variations of allometric shape were visualized through Thin-Plate-Spline (TPS) deformation grids representing minimum and maximum CAC scores. And shape configurations at CAC extremes were generated with shape.predictor function in *geomorph* package.

Decision tree classifier

For inferring and refining the taxonomic keys for three *Miniopterus* species in China, a decision tree classifier was implemented with R package *rpart* (Therneau et al., 2015). With its typical tree-like structure, this supervised learning model may predict outcomes based upon predefined target results. Decision tree consists of root nodes, branches and leaf nodes. Data were evaluated by traversing a path from root to a certain leaf node according to the node threshold. For algorithm settings in this study, random number generator was set to 1 234 and the dataset was randomized into the sets of training (70%) and test (30%). The model included a total of 169 samples, i.e., *M. fuliginosus* (*n*=62), *M. magnater* (*n*=63) and *M. pusillus* (*n*=44). Each sample consisted of 5 external and 17 craniodental morphological measurements. For assessing the classifier's predictive accuracy and overall performance, the following metrics of accuracy, receiver operating characteristic curve (ROC), area under receiver operating characteristic curve (AUC), sensitivity (true positive rate), specificity (true negative rate) and balanced accuracy (average of sensitivity and specificity) were calculated.

RESULTS

Phylogeny

ML phylogenetic tree, validated by Bayesian phylogenetic tree, uncovered three distinct monophyletic lineages of *M. fuliginosus* (this study, *n*=69; NCBI-nt, *n*=26), *M. magnater* (this study, *n*=54; NCBI-nt, *n*=32) and *M. pusillus* (this study, *n*=3; NCBI-nt, *n*=12) (Figure 1). *COI*-based phylogenetic inference placed *M. fuliginosus* as a well-supported sister taxon to *M. magnater*, forming a clade sister to *M. phillipsi* (clade I). *M. pusillus* was identified as a sister taxon to *M. medius* from Malaysia and clusters with *M. medius* (from Malaysia & Lao PDR), *M. australis* and *M. srinii* clade (clade II). These two major clades were robustly supported as a sister group (Figure 1). Notably, *M. medius* and *M. natalensis* exhibited paraphyletic relationships within phylogeny and Kenya region showed exceptionally high diversity (Figure 1).

Mean genetic distances among three *Miniopterus* species were as follows: 6.48% (*M. fuliginosus*–*M. magnater*), 13.73% (*M. fuliginosus*–*M. pusillus*) and 14.34% (*M. magnater*–*M. pusillus*) (Supplementary Table S3). Pairwise genetic distances between *M. fuliginosus* and *M. magnater* to *M. phillipsi* were 9.17%, while *M. pusillus* and *M. medius* (from Malaysia) diverged by 7.72% with 9.13% divergence to *M. srinii*, *M. medius* (from Malaysia & Lao PDR) and *M. australis* group. Clade I/II exhibited a mean pairwise genetic distance of 14.72% (Supplementary Table S4).

Intralineage divergences among three *Miniopterus* species were as follows: 0.67% within *M. fuliginosus* (ranging from 0 to 2.74%), 0.73% within *M. magnater* (ranging from 0 to 2.14%) and 1.09% within *M. pusillus* (ranging from 0 to 2.74%) (Supplementary Table S3). Among inter-population comparisons within each species, the highest average genetic divergences were noted in the following populations: *M. fuliginosus* from Taiwan Island (HM540882, ranging from 1.58% to 2.74%), *M. magnater* from Guangxi (HM540895, ranging from 0.89% to 1.41%) and *M. pusillus* from Vietnam (HM540924, HM540917, HM540923, ranging from 1.37% to 1.74%) (Supplementary Table S4).

Species distribution pattern of three *Miniopterus* in China

The current distribution pattern of *Miniopterus* species in China is shown in Figure 2. *Miniopterus fuliginosus* is widely distributed in 20 provinces/areas, including Beijing, Hebei, Henan, Shandong, Shaanxi, Anhui, Hubei, Sichuan, Chongqing, Hunan, Jiangxi, Zhejiang, Yunnan, Guizhou, Guangxi, Guangdong, Fujian, Hong Kong, Hainan Island and Taiwan Island. In comparison, *M. magnater* tends to be more restricted, localized to 6 provinces/areas in South China, including Yunnan, Guangxi, Guangdong, Hong Kong, Fujian and Hainan Island. *Miniopterus pusillus* is spotted across 7 provinces/areas of Yunnan, Guangxi, Guangdong, Hong Kong, Macau, Fujian and Hainan Island.

ESDMs for three *Miniopterus* species demonstrated strong predictive performance, as indicated by consistently high AUC, sensitivity, specificity, prop.correct values, low omission rate values and reasonable Kappa values (Table 1). And potential habitat maps revealed distinct distribution patterns for each species (Figure 3A–C). *Miniopterus fuliginosus* exhibited widespread habitat suitability across middle tropical to south temperate zone. And the highest suitability was concentrated in mountain areas of South China (>0.6) (Figure 3A). The habitat of *M. magnater* is predominantly located in South China, particularly concentrated in tropical and southern subtropical regions (>0.6) (Figure 3B). *Miniopterus pusillus* shares significant habitat overlap with *M. magnater*, except in western Nanling Mountains, Wuyi Mountains and eastern Hengduan Mountains where *M. pusillus* displayed higher probability scores (>0.6) (Figure 3B,

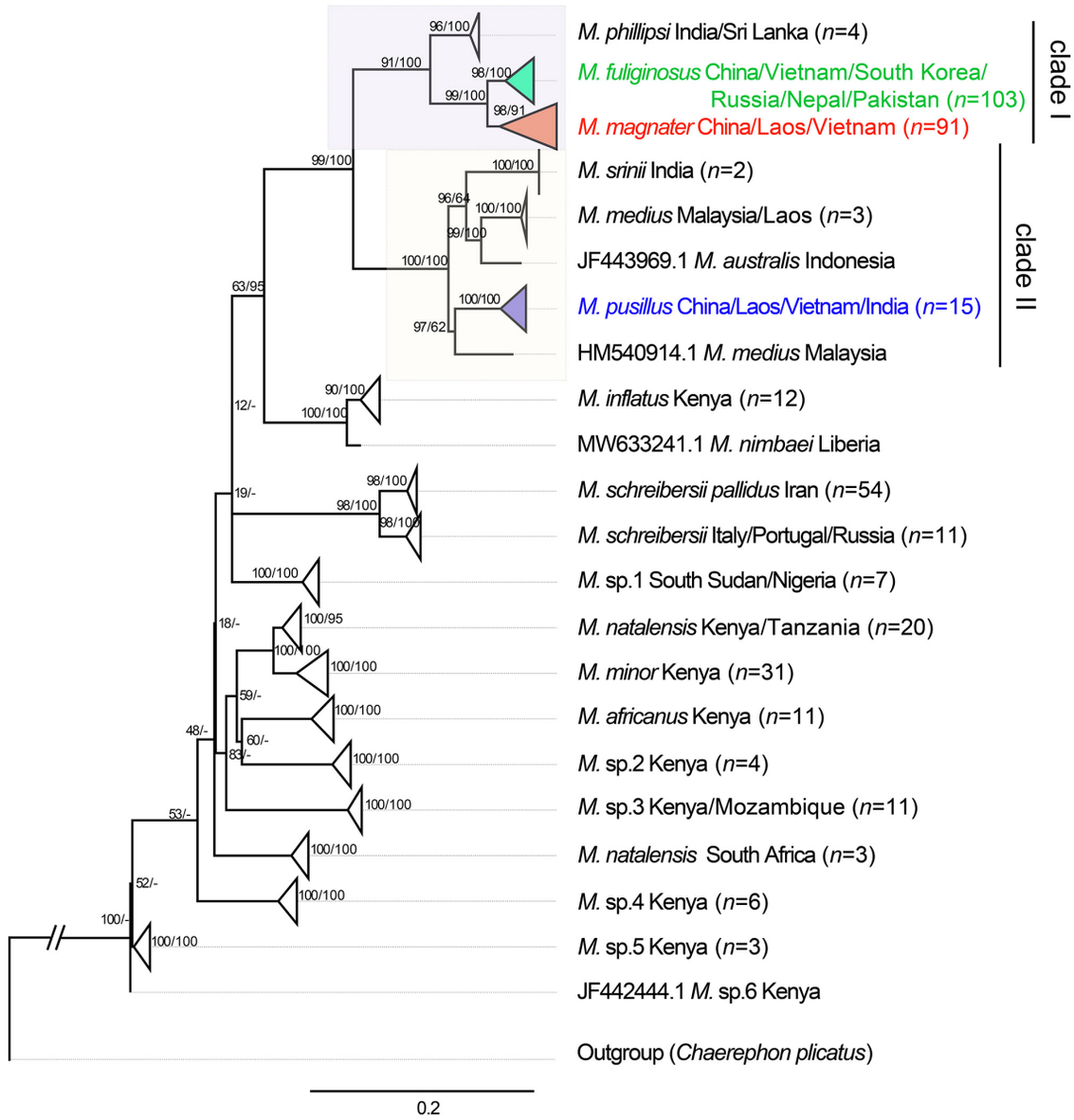

Figure 1 Phylogenetic tree was based upon maximum likelihood (ML) analysis of *COI* sequences and validated by Bayesian analysis

Values at the nodes and branches denoted posterior probability of ML and Bayesian analyses, respectively (%). Green branch: *M. fuliginosus*; red branch: *M. magnater*; blue branch: *M. pusillus*. (*n*: number of sequences).

C). Notably, southern Xizang demonstrated high suitability for all three *Miniopterus* species (Figure 3A–C).

The environmental factors contributing to potential habitats of three *Miniopterus* species varied greatly (Figure 3D, E). For *M. fuliginosus*, key factors included precipitation seasonality (bio15), precipitation of the warmest quarter (bio18, with a preference of 500–1 000 mm) and precipitation of the coldest quarter (bio19, preferring areas over 120 mm) (Figure 3D, E). As for *M. magnater*, temperature seasonality (bio4, negatively correlated with habitat preference) and precipitation of the driest month (bio12, positively correlated with habitat preference) were primary contributors (Figure 3D, E). For *M. pusillus*, annual precipitation (bio12, favoring higher rainfall) and precipitation of the warmest quarter (bio18, positively associated with habitat preference) were critical (Figure 3D, E). Response curves indicated that *M. fuliginosus* exhibited broader adaptability than the other two species (Figure 3E). All three species demonstrated a preference for lower elevation areas, although elevation did not appear to limit habitat suitability for *M. fuliginosus* (suitability response scores >0.5, Figure 3E).

Morphometric differences

ANOVAs of external and skull linear measurements revealed significant differences among three species (Table 2). *Miniopterus pusillus* exhibited markedly smaller body and skull sizes (P<0.001, Table 2). In contrast, *M. magnater* was larger than *M. fuliginosus*, although considerable morphological overlap existed between the two species (P<0.001, Table 2). The two species differed significantly, except for HFL (P>0.05, Table 2). ANCOVAs, with GLS as a covariate, revealed significant differences among three species, as well as CBL, PL, BCH, LPB, C^1C^1, M^3M^3, C^1M^3, C_1M_3, HCPM, ML and M_3M_3 between the two morphologically similar species. Significant differences also existed in ZB, BCH, MW, M^3M^3, C^1M^3 and ML between *M. fuliginosus* and *M. pusillus* and CBL, ZB, MW, C^1C^1, M^3M^3, C^1M^3, C_1M_3, HCPM and ML between *M. magnater* and *M. pusillus* (Table 2). The PCA results of skull parameters demonstrated that three species

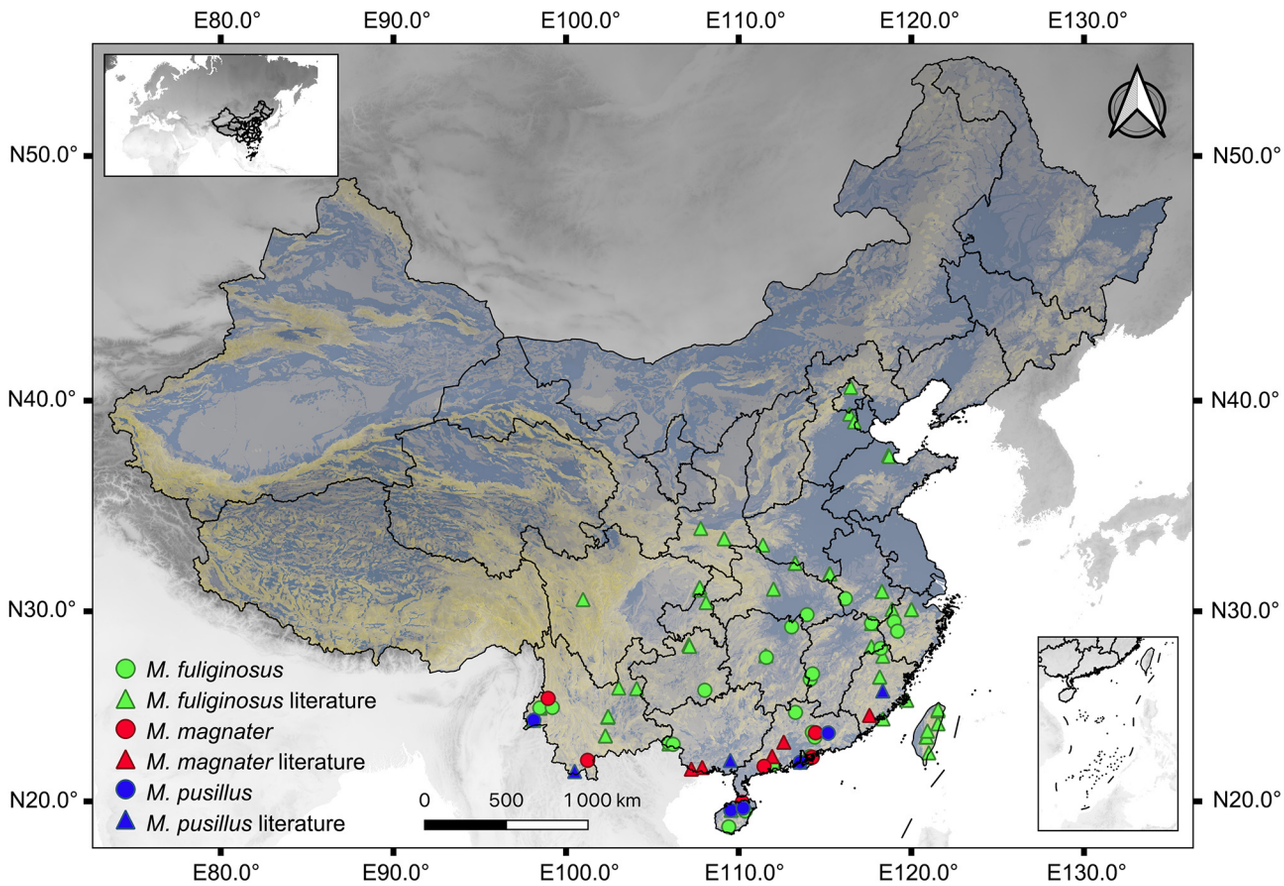

Figure 2 Illustrative map of domestic occurrence points for three *Miniopterus* in China

Species were denoted with different colors and data sources different symbols; Supplementary Table S2 depicted geographic coordinates of localities; background Map: Geomorphological types of China, downloaded from Resource and Environmental Science Data Platform.

Table 1 Ensemble species distribution model evaluation of three *Miniopterus* species

	AUC	Omission rate	Sensitivity	Specificity	prop.correct	Kappa
Miniopterus fuliginosus	0.9229	0.1342	0.8847	0.8604	0.8658	0.6924
Miniopterus magnater	0.9206	0.0597	0.9406	0.9172	0.9403	0.6662
Miniopterus pusillus	0.8532	0.0477	0.8604	0.9377	0.9523	0.6420

AUC, area under receiver operating characteristic curve; Kappa, Cohen's Kappa; prop.correct, proportion of correctly predicted occurrences.

were predominantly distinguished by their PC1 scores (PC1 90.74%, Figure 4). *Miniopterus magnater* displayed a lower PC1 score. And *M. fuliginosus* occupied an intermediate score with some overlap with *M. magnater* while *M. pusillus* had a higher PC1 score, distinctly separated from the other two species (Figure 4). Factor loading analysis indicated that variance in PC1 was primarily associated with overall skull elements (Table 2).

The results of SSD MANOVA demonstrated that *M. magnater* displayed male-biased SSD (P=0.009) whereas male *M. fuliginosus* was slightly larger than female counterpart with no significant differentiation (P=0.179). Despite significant male-biased SSD across various skull linear measurements for both *M. magnater* and *M. fuliginosus* (Supplementary Table S5), PCA plot revealed considerable overlap between genders in both species (Figure 4). The results of MANOVA indicated significant geographical variations within all three species (Supplementary Table S5). *Miniopterus fuliginosus* varied across 10 provinces/areas while *M. magnater* and *M. pusillus* differed across 4 provinces/areas (Supplementary Table S5). However, PCA plots of linear measurements did not distinctly illustrate patterns of sexual dimorphism or geographical variations within each species (Figure 4).

Geomorphometric variations

As for cranial and mandibular shape variations among three *Miniopterus* species, significant differences existed in centroid size and shape (Procrustes ANOVAs, P<0.001). *M. magnater* had a slightly larger centroid size than *M. fuliginosus* whereas *M. pusillus* displayed a significantly smaller centroid size. The scatter plots of the first two PC axes (cranium: PC1, 17.9% and PC2, 13.2%; mandible: PC1, 23.8% and PC2, 11.7%) illustrated potential patterns of shape change among species. However, these plots did not distinctly display sexual dimorphism or geographical variation patterns within each species.

The average shape of cranium was approximated to *M. fuliginosus* (GZHU 17009). Characterized by lower PC2 scores, *M. pusillus* exhibited an inflated forehead, braincase and tympanic bulla, shorter teeth and a narrower and upturned rostrum as compared to mean shape. Conversely, *M. magnater* exhibited higher PC2 scores, indicating a wider, stronger rostrum, a broader, elongated palate, longer teeth, a deflated forehead, braincase and tympanic bullae relative to

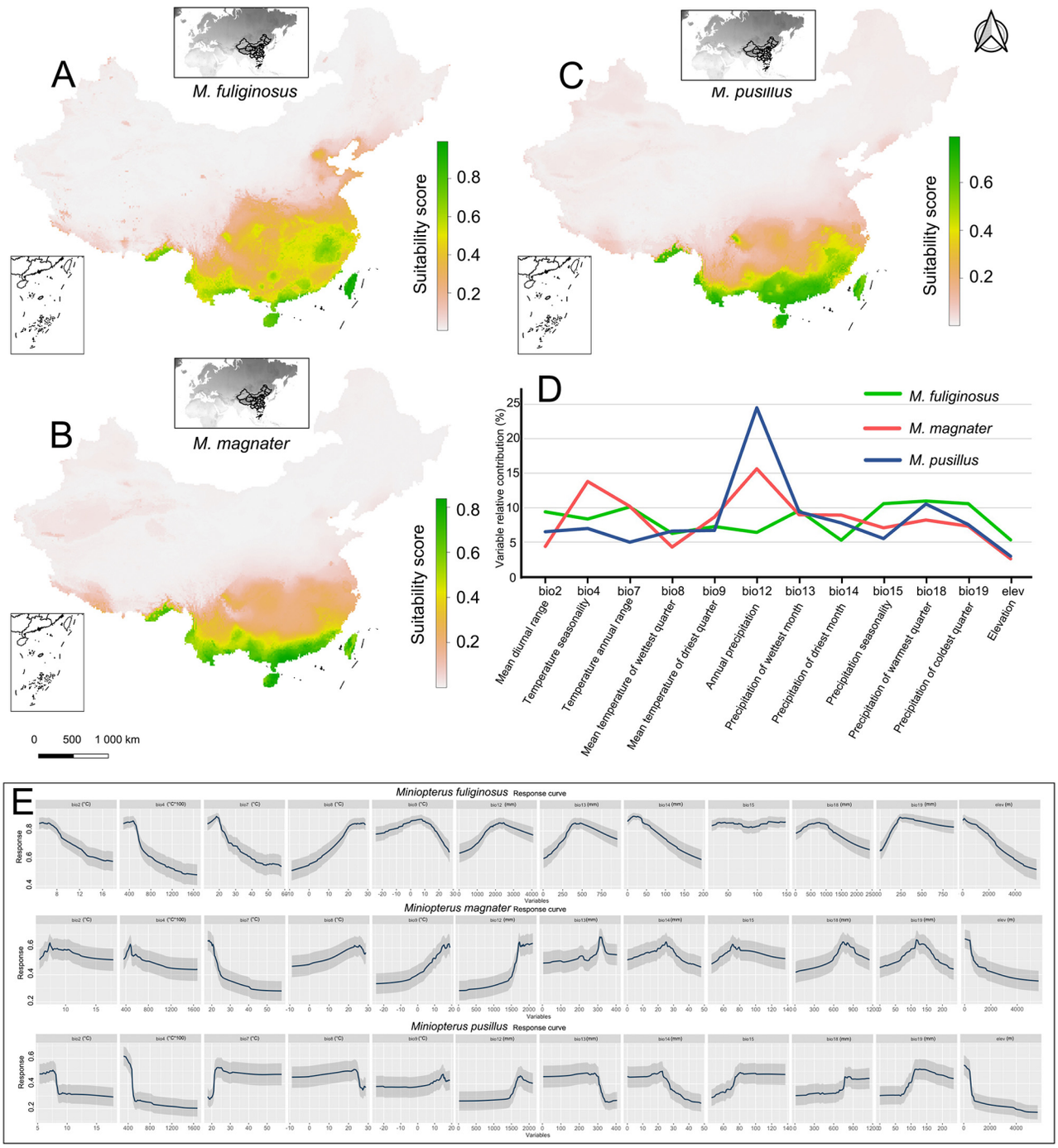

Figure 3 The ensemble species distribution model (ESDM) of three *Miniopterus* species

A: *M. fuliginosus*; B: *M. magnater*; C: *M. pusillus*; D: Stack line plot of the contribution of each environmental variable (species are designated with different colors); E: Response curves illustrating the relationship between species distributions and environmental variables.

mean shape (Figure 5A). As for mandible, the average shape was approximated to *M. fuliginosus* (GZHU 17132). *Miniopterus pusillus* was characterized by higher PC1 and lower PC2 scores, correlated with an elongated, thinner mandible and shorter teeth than *M. fuliginosus*. Conversely, *M. magnater* exhibited lower PC1 and higher PC2 scores, indicating a wider, stronger mandible and a well-developed canine as compared to *M. fuliginosus* (Figure 5B).

The results of CVA displayed an overall classification accuracy of 95.58% (cranium, Kappa statistic: 0.9288) and 90.48% (mandible, Kappa statistic: 0.8483), respectively. The scatter plots of two CV axes (cranium: CV1, 78.41%; CV2, 21.59%, mandible: CV1, 83.34%; CV2, 16.66%) revealed significant shape differences among three species (Figure 5C, D), without sexual dimorphism and geographical variation pattern. Cranial CV1 scores helped to distinguish *M. pusillus* by its inflated braincase, shorter teeth and narrower and upturned rostrum as compared to *M. fuliginosus* and *M. magnater*. *Miniopterus magnater* was characterized by higher cranial CV2 scores, a slightly deflated braincase, longer teeth and elongated rostrum as compared to *M. fuliginosus* (Figure 5C). Mandibular CV1 scores helped to distinguish *M. pusillus* by its slightly elongated, narrower mandible as compared to *M. fuliginosus* and *M. magnater*. *Miniopterus magnater* was characterized by a shorter, wider mandible as compared to *M. fuliginosus* (low mandibular CV2 score) with

Table 2 External and craniodental measurements (mm) for morphometric analysis of three *Miniopterus* species found in China

	M. fuliginosus (*n*=61)			*M. magnater* (*n*=59)			*M. pusillus* (*n*=41)			ANOVA *P* values			ANCOVA(GLS) *P* values			PCA		
	Mean ± SD	Range	*n*	Mean ± SD	Range	*n*	Mean ± SD	Range	*n*	*M. fuliginosus*-*M. magnater*	*M. fuliginosus*-*M. pusillus*	*M. magnater*-*M. pusillus*	*M. fuliginosus*-*M. magnater*	*M. fuliginosus*-*M. pusillus*	*M. magnater*-*M. pusillus*	PC1(90.74%)	PC2(2.57%)	PC3(1.60%)
HBL	54.2 ± 4.5	36.7 – 63.0	52	57.6 ± 3.7	45.7 – 66.4	56	42.3 ± 4.8	33.8 – 54.0	40	<0.001	<0.001	<0.001						
TL	54.0 ± 6.5	40.4 – 66.4	58	57.7 ± 4.9	44.0 – 67.6	54	47.3 ± 4.1	39.5 – 54.6	37	<0.001	<0.001	<0.001						
EL	10.9 ± 1.3	8.0 – 13.7	59	11.9 ± 1.3	8.6 – 14.6	56	9.2 ± 1.1	6.0 – 11.9	39	<0.001	<0.001	<0.001						
HFL	10.2 ± 1.1	6.9 – 14.3	59	9.9 ± 1.3	7.2 – 11.9	56	8.7 ± 0.7	7.3 – 10.5	40	0.458	<0.001	<0.001						
FAL	48.7 ± 1.8	41.3 – 52.2	59	49.8 ± 1.3	43.5 – 52.4	56	41.3 ± 0.8	39.5 – 43.3	40	<0.001	<0.001	<0.001						
TibL	20.5 ± 0.7	19.1 – 21.8	39	21.5 ± 0.8	20.3 - 23.5	41	17	NA	1	<0.001	–	–						
GLS	16.30 ± 0.44	15.57 – 17.17	59	16.93 ± 0.25	16.2 – 17.46	59	14.08 ± 0.24	13.58 – 14.46	41	<0.001	<0.001	<0.001	–	–	–	-0.2517	-0.0529	-0.0367
OCL	14.62 ± 0.48	13.8 – 15.69	59	15.23 ± 0.32	14.62 – 15.97	59	12.45 ± 0.23	11.84 – 12.77	41	<0.001	<0.001	<0.001	0.3066	0.0864	0.0874	-0.2503	-0.0900	0.0516
CBL	15.52 ± 0.49	14.62 – 16.63	56	16.18 ± 0.29	15.55 – 16.88	57	13.28 ± 0.24	12.69 – 13.62	41	<0.001	<0.001	<0.001	0.0373	0.0532	0.0250	-0.2513	-0.0873	0.0251
PL	8.30 ± 0.42	7.53 – 9.20	58	8.93 ± 0.38	8.05 – 9.66	57	6.95 ± 0.43	6.11 – 7.85	41	<0.001	<0.001	<0.001	0.0021	0.9560	0.3263	-0.2361	0.5006	0.1047
ZB	9.15 ± 0.27	8.54 – 9.88	59	9.53 ± 0.22	9.01 – 10.05	57	7.74 ± 0.18	7.40 – 8.01	38	<0.001	<0.001	<0.001	0.0701	0.0023	0.0024	-0.2499	-0.1538	-0.0774
BB	8.15 ± 0.21	7.72 – 8.67	61	8.46 ± 0.22	8.09 – 9.62	59	7.38 ± 0.14	7.09 – 7.59	41	<0.001	<0.001	<0.001	0.1040	0.3824	0.8785	-0.2432	-0.0303	0.0504
BCH	7.18 ± 0.25	6.67 – 7.79	55	7.61 ± 0.22	6.80 – 8.14	59	6.45 ± 0.17	6.12 – 6.78	41	<0.001	<0.001	<0.001	0.0002	0.0363	0.6945	-0.2401	-0.0656	0.2112
MW	9.02 ± 0.23	8.51 – 9.48	59	9.33 ± 0.18	8.94 – 9.70	59	7.97 ± 0.17	7.64 – 8.48	41	<0.001	<0.001	<0.001	0.1940	0.0440	0.0414	-0.2475	-0.1119	-0.0625
IOW	4.13 ± 0.20	3.83 – 4.85	61	4.24 ± 0.12	3.95 – 4.66	59	3.74 ± 0.10	3.53 – 3.93	41	<0.001	<0.001	<0.001	0.2650	0.1160	0.1040	-0.2211	-0.2790	0.7814
LPB	6.39 ± 0.42	5.44 – 7.22	61	6.95 ± 0.42	5.93 – 7.73	59	5.51 ± 0.41	4.83 – 6.38	41	<0.001	<0.001	<0.001	0.0221	0.1190	0.6323	-0.2187	0.7355	0.1432
C^1C^1	4.90 ± 0.20	4.50 – 5.42	61	5.23 ± 0.16	4.77 – 5.53	59	4.03 ± 0.10	3.86 – 4.22	38	<0.001	<0.001	<0.001	0.0005	0.0836	0.0111	-0.2492	-0.0789	-0.0733
M^3M^3	6.93 ± 0.27	6.40 – 7.62	61	7.46 ± 0.18	6.66 – 7.85	59	5.65 ± 0.12	5.36 – 5.89	41	<0.001	<0.001	<0.001	<0.0001	0.0077	<0.0001	-0.2511	-0.0563	-0.1045
C^1M^3	6.28 ± 0.25	5.86 – 6.92	59	6.71 ± 0.18	6.30 – 7.67	58	5.16 ± 0.11	4.86 – 5.39	41	<0.001	<0.001	<0.001	<0.0001	0.0006	<0.0001	-0.2487	0.0405	-0.0272
C_1M_3	6.95 ± 0.27	6.52 – 7.66	59	7.41 ± 0.21	6.63 – 7.86	58	5.78 ± 0.18	5.35 – 6.16	41	<0.001	<0.001	<0.001	0.0003	0.2096	0.0278	-0.2477	-0.0293	-0.1106
HCPM	4.85 ± 0.25	4.14 – 5.43	57	5.13 ± 0.26	4.58 – 5.72	57	4.20 ± 0.12	3.95 – 4.42	41	<0.001	<0.001	<0.001	0.0025	0.1882	0.0396	-0.2254	0.0770	-0.3844
ML	12.19 ± 0.38	11.58 – 13.22	60	13.04 ± 0.32	11.55 – 13.58	59	10.21 ± 0.26	9.57 – 10.7	41	<0.001	<0.001	<0.001	<0.0001	0.0007	<0.0001	-0.2501	-0.0090	-0.0910
M_3M_3	4.76 ±	4.26 –	56	5.15 ±	4.22 –	57	3.87 ±	3.57 –	38	<0.001	<0.001	<0.001	0.0009	0.0955	0.1501	-0.2368	-0.2298	-0.3331

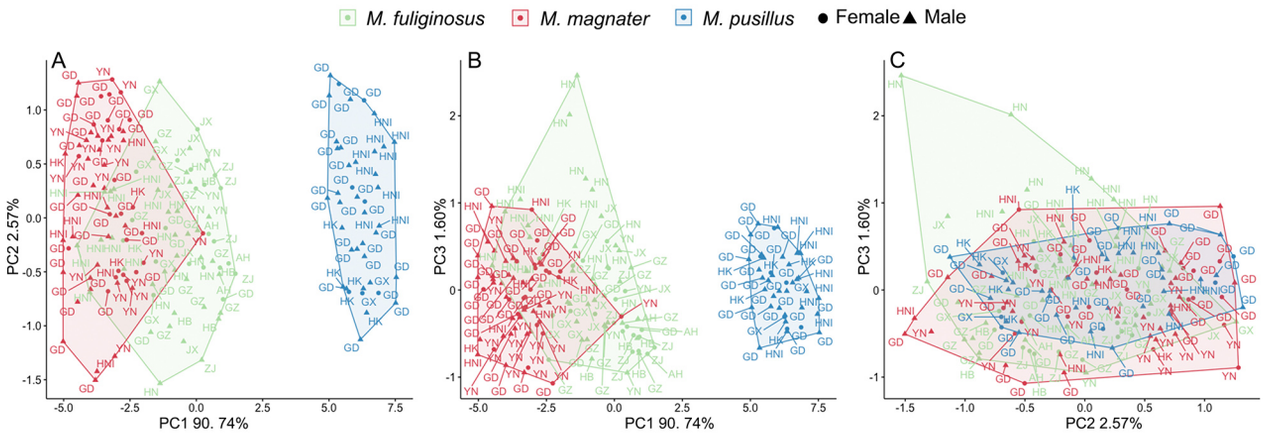

Figure 4 Principal component analysis (PCA) scatter plots depicting craniodental variations among three *Miniopterus* species

Axes denoted principal component (PC) 1–3 and percentage of variation explained by each. AH, Anhui; GD, Guangdong; GX, Guangxi; GZ, Guizhou; HB, Hubei; HK, Hong Kong; HN, Hunan; HNI, Hainan Island; JX, Jiangxi; YN, Yunnan; ZJ, Zhejiang; species were designated with different colors, and gender was highlighted with different symbols.

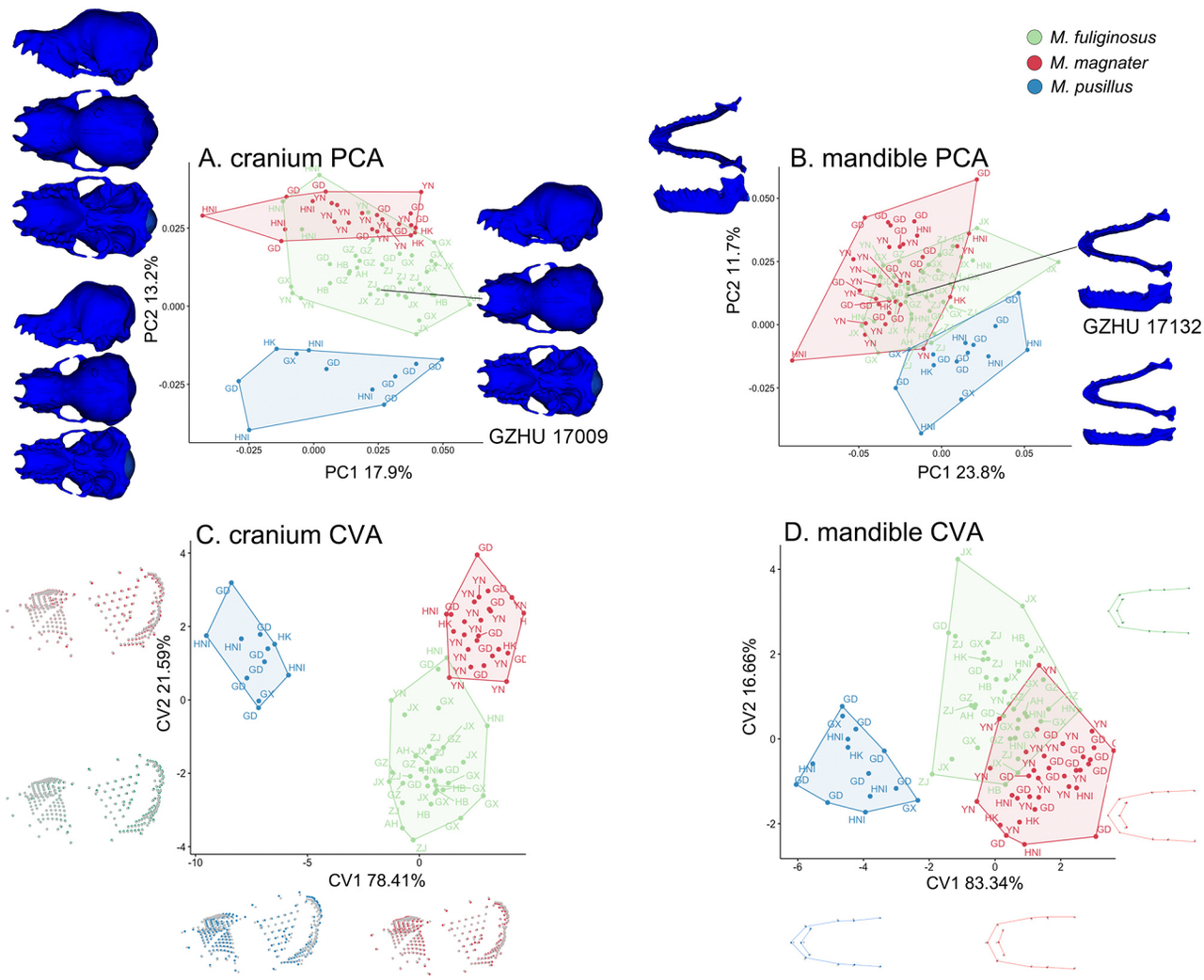

Figure 5 Scatter plots illustrating 3D skull model principal component analysis (PCA, A: cranium; B: mandible) and canonical variate analysis (CVA, C: cranium; D: mandible) of three *Miniopterus* species based upon skull geometric morphometry

Axes denoted principal component (PC) 1–2 and canonical variate (CV) 1–2 and percentage of variation explained by each. AH, Anhui; GD, Guangdong; GX, Guangxi; GZ, Guizhou; HB, Hubei; HK, Hong Kong; HN, Hunan; HNI, Hainan Island; JX, Jiangxi; YN, Yunnan; ZJ, Zhejiang; species were illustrated with different colors.

minimal overlap between *M. fuliginosus* and *M. magnater* (Figure 5D).

After correcting 3D skull model using GLS, CAC analysis indicated that three *Miniopterus* species formed three main

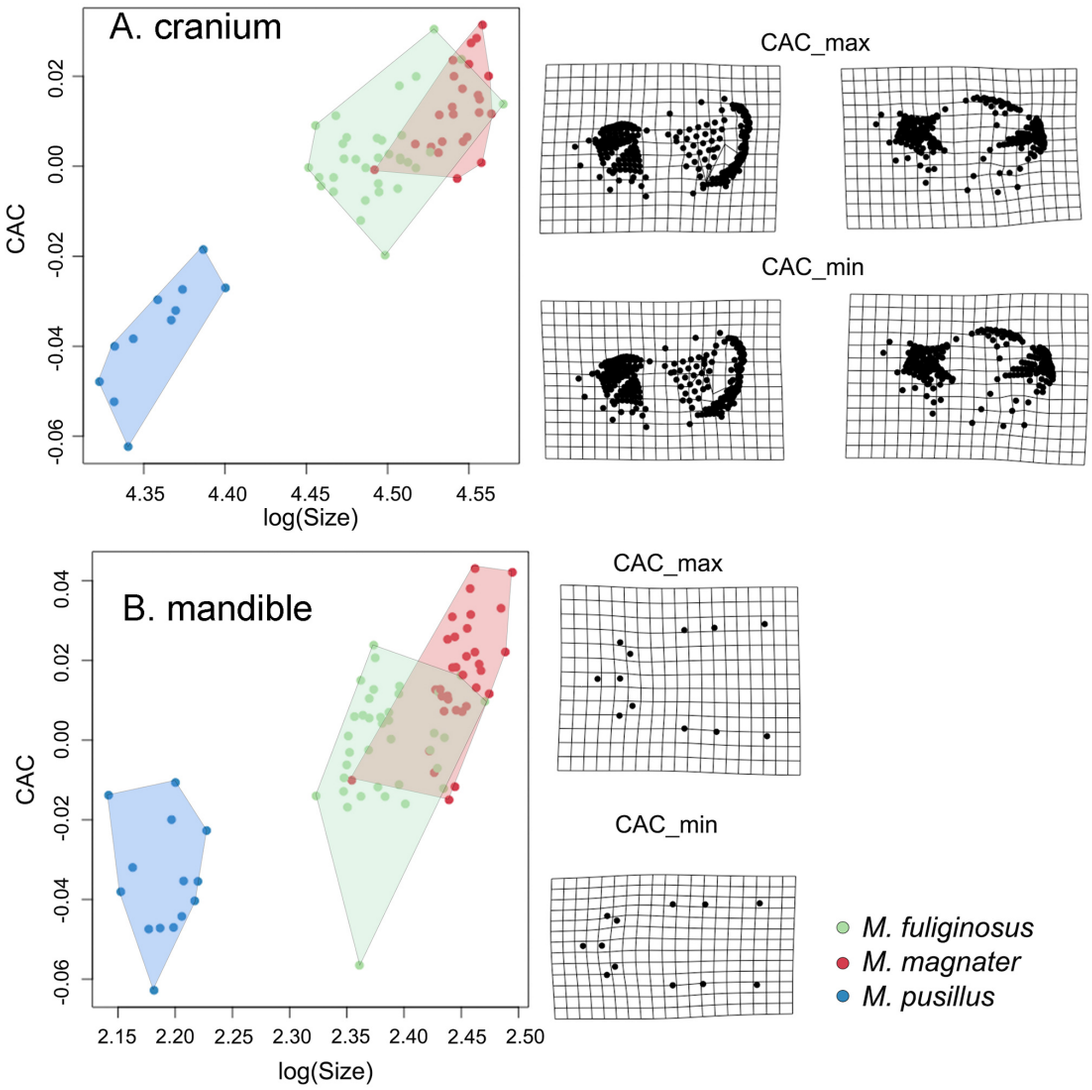

Figure 6 Scatter plots of shape–size covariation of three *Miniopterus* 3D skull models

Logged centroid sizes (log (Size)) and common allometric components (CAC, GLS as a metric represented as skull size) resided on x- and y-axis, respectively. TPS deformation grids denoted shapes at CAC extremes (versus sample mean). Species were illustrated with different colors.

groups, both cranial and mandibular shapes (Figure 6). *Miniopterus pusillus* stood apart from the other two species with lower CAC scores and smaller centroid sizes, characterized by a slightly inflated braincase and tympanic bullae, a compact and upturned rostrum (Figure 6A) and a narrow mandible, with anterior part of mandible was relatively spherical (Figure 6B). In contrast, *M. magnater* displayed the highest CAC scores and largest centroid sizes, with slightly spherical and wider rostrum, deflated braincase and tympanic bullae (Figure 6A) and a wider mandible (Figure 6B). *M. fuliginosus* overlapped with *M. magnater*. However, there was an overall trend of smaller CAC values and centroid sizes (Figure 6A, B).

Decision tree classifier

In external aspect, decision tree classifier using five body linear elements successfully differentiated three *Miniopterus* species. Root nodes were determined by FAL and HBL with the thresholds of 43 mm and 57 mm, respectively. This created three branches: One for FAL<43 mm (mainly *M. pusillus*, *n*=31), a second for FAL≥43 mm and HBL<57 mm (*M. fuliginosus*, *n*=34; *M. magnater*, *n*=12; *M. pusillus*, *n*=2), and a third for FAL≥43 mm and HBL≥57 mm (*M. magnater*, *n*=31; *M. fuliginosus*, *n*=11) (Figure 7A). This classifier achieved an overall accuracy of 60.9% with high accuracies for *M. pusillus* (96.9%) and moderate performance for *M. fuliginosus* (70.8%) and *M. magnater* (73.8%) (Figure 7C).

Based upon 17 skull linear elements, root nodes were determined by BB and M^3M^3, assuming the threshold values of 7.7 mm and 7.2 mm. This resulted in three branches: One for BB<7.7 mm (mainly *M. pusillus*, *n*=33), a second for BB≥ 7.7 mm and M^3M^3<7.2 mm (mainly *M. fuliginosus*, *n*=39) and a third for BB≥7.7 mm and M^3M^3≥7.2 mm (mainly *M. magnater*, *n*=45) (Figure 7B). The classifier yielded an overall accuracy of 89.3% with perfect performance for *M. pusillus* (100%) and high accuracies for *M. fuliginosus* (97.5%) and *M. magnater* (83.3%) (Figure 7D).

DISCUSSION

Reconfirmation of three *Miniopterus* species in China

Phylogenetic tree has confirmed the presence of three *Miniopterus* species of *M. fuliginosus*, *M. magnate* and *M. pusillus* in China. Mitochondrial (*COI* gene) phylogeny relationships among three *Miniopterus* species were

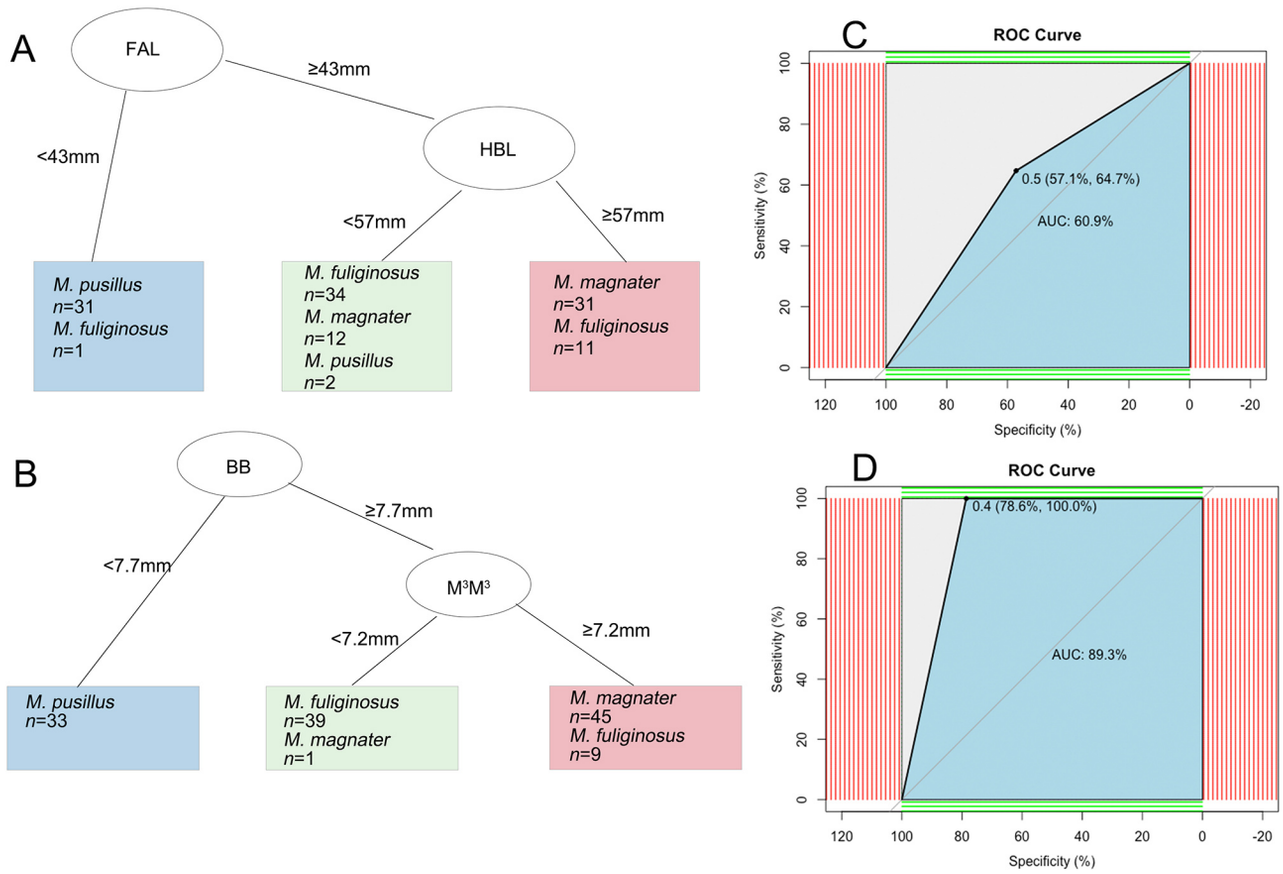

Figure 7 Decision tree classifiers of potential parameters for species identification among three *Miniopterus* species

A: 5 external elements; B: 17 craniodental elements; C: Accuracy test of external elements decision tree classifier; D: Accuracy test of craniodental elements decision tree classifier; species were illustrated with different colors; *n*: number of samples.

consistent with those reported by Kusuminda et al. (2022). No distinct geographical pattern has been observed within the species of both *M. fuliginosus* and *M. magnater* across China and Eurasian Plate. It implied that extensive genetic exchanges might occur across a broad range for these two species, likely facilitated by their long-distance migratory capabilities (Amengual et al., 2007; Li et al., 2015; Rodrigues & Palmeirim, 2008; Tian et al., 2004). Interestingly, pairwise genetic distances revealed that *M. fuliginosus* sequence from Taiwan Island (HM540882.1; ~2% at species level, Mou et al., 2024) exhibited significantly larger values than other regions, implying potential geographical genetic variations (Supplementary Table S4). Further phylogenetic studies are warranted for exploring these variations in more details.

Additionally, *M. magnater* population from China may represent a distinct cryptic species or subspecies to the population from New Guinea, type locality of *M. magnater*. Despite considerable morphological overlapping (Supplementary Table S6), the Chinese population, previously recognized as "*M. schreibersii* China", exhibited a slightly smaller size. However, substantial molecular divergence existed between these two populations, as evidenced by mitochondrial NADH dehydrogenase subunit 2 (*ND2*) gene (Appleton et al., 2004; Li et al., 2015). Furthermore, our findings suggest that the *M. pusillus* population from China was larger than Nicobar Islands population (India, type locality of *M. pusillus*), but slightly smaller than the population from northeastern India in terms of body and skull size (Supplementary Table S6). Therefore, more detailed phylogenetic and morphological comparative studies are required for further clarifying the taxonomy of these species, with a particular focus on population variations from New Guinea and Nicobar Islands.

Current distribution pattern of three *Miniopterus* species

The geographic distributions of three *Miniopterus* species in China were confirmed through molecular phylogenetic evidence and a comprehensive literature review. Notably, all three *Miniopterus* species co-occur in southern China, specifically in Yunnan, Guangxi, Guangdong, Hainan Island and Fujian (Figure 2). The distribution ranges of these species extend beyond China. *Miniopterus fuliginosus* has been spotted in Korean Peninsula, southern Russia (Far East), Japan, northern India, Nepal, Myanmar, Lao PDR, Vietnam, northeastern Afghanistan and northern Pakistan (Endo et al., 2019; Ibáñez & Juste, 2019; Kusuminda et al., 2022; Li et al., 2015; Thomas et al., 2013). *Miniopterus magnater* is found throughout Southeast Asia (Thailand, Myanmar, Lao PDR, and Vietnam), India, Sunda Islands (Sumatra, Borneo, Java, Nusa Penida, and Timor), Central Moluccas (Seram and Ambon Islands) and New Guinea (Ibáñez & Juste, 2019; Kusuminda et al., 2022, Li et al., 2015). *Miniopterus pusillus* is distributed in Nepal, northern India and Southeast Asia (Thailand, Myanmar, Lao PDR, Vietnam, and Cambodia), as well as part of insular Southeast Asia (Nicobar Island, Sumatra, Java, Sulawesi, Lesser Sundas, and Moluccas) (Ibáñez & Juste, 2019; Srinivasulu & Srinivasulu, 2023). While *M. magnater* and *M. pusillus* closely overlap in China, they exhibited global differences, including in Nepal, Cambodia, Indonesian Archipelago, and New Guinea. It is essential to

emphasize that accurate species distributions in these areas require re-evaluation and confirmation through phylogenetic and morphological evidence, especially given the historical misclassification of these morphologically similar groups as *M. schreibersii*.

Furthermore, species name "*Miniopterus schreibersii*" continues to be erroneously used in China per older taxonomic classifications (Dong et al., 2023; Liang et al., 2017; Su et al., 2023; Wang et al., 2023). Notably, *M. schreibersii*, endemic in Europe, exhibited a smaller average forearm length (mean FAL of 45.0 mm; Lisón et al., 2017) than *M. magnater* (mean FAL of 49.8 mm) and *M. fuliginosus* (mean FAL of 48.7 mm). According to current taxonomy, the entities previously identified as "*M. schreibersii*" in China were probably *M. fuliginosus* or *M. magnater*. Regarding Xinjiang area, we recommended re-identifying "*M. schreibersii*" as *M. fuliginosus* (Dong et al., 2023), based upon reported mean peak frequencies of approximately 51.5 kHz (Wu et al., 2020) representing the westernmost distribution record in China. The classification of "*M. schreibersii*" in Macau (Liang et al., 2017) remains controversial due to the coexistence of three *Miniopterus* species in adjoining areas of Hong Kong and Guangdong.

Potential suitable habitat of three *Miniopterus* species

ESDM indicated that the highly suitable habitats for three *Miniopterus* species largely overlapped in South China (Figure 3). These areas of high suitability coincided with identified hotspots for terrestrial mammals (Chi et al., 2020; Sun et al., 2022). Historically, these regions served as Quaternary refuges (Rahbek et al., 2019), providing stable climates and complex topography for various species (He & Jiang, 2014, Sun et al., 2022, Zhang et al., 2020). However, pronounced discrepancies existed between ESDM prediction and actual distribution (Figure 2, Figure 3A–C), particularly in southern Qinghai-Xizang Plateau (where all three species showing high distribution probabilities), Taiwan Island (where *M. magnater* and *M. pusillus* with high distribution probabilities), Hengduan Mountains (where *M. pusillus* with a high probability) and area surrounding Beijing (where *M. fuliginosus* with a relatively low distribution probability). These inconsistencies implied at a potential underestimation of biodiversity in regions. Additionally, potential suitable habitat of *M. fuliginosus* appears to be underrated. While *M. magnater* and *M. pusillus* tend to inhabit tropical or subtropical regions. Due to the limitations of latitude, rainfall and temperature (Figure 3B–E), these factors have been closely associated with bat hibernation patterns, insect diversity and food availability (Arthur et al., 2014; Bronrier et al., 1999; Rebelo et al., 2010; Webb et al., 1996). Moreover, the discrepancies between predicted and actual distributions highlighted certain limitations of the model, such as ignoring interspecific competition, specific geographic barriers (e.g., high mountains) and impulse or capabilities of migration and dispersal capabilities of the species (Burke et al., 2019; Salinas-Ramos et al., 2021). These discrepancies implied that the suitable habitats for these species may be gradually shrinking as intensity, frequency and duration of extreme weather events have spiked globally (Ancillotto et al., 2021; Festa et al., 2023), emphasizing the urgency of proactive conservation efforts to mitigate habitat compression. Given the sensitivity of bats to climate change, understanding their responses is crucial for conducting vulnerability assessments and developing effective conservation strategies. Furthermore, loss of these insectivorous bat pest suppression ecosystem service in abandoned regions could have potentially negative consequences for agriculture, forests and human health (Smeraldo et al., 2021). This study aims to provide a comprehensive background reference for the spatial distribution of *Miniopterus* bats, offering critical insights to guide their conservation.

Additionally, divergent distribution patterns among these three *Miniopterus* species hinted at varying historical biogeographic processes. *Miniopterus fuliginosus* occupied a broader latitudinal region across the north-south axis, likely implying its association with Quaternary glacial refuge in China (Fu & Wen, 2023). During this period, ancestral *M. fuliginosus* may have occupied more northern refuges than the other two species (Kimprasit et al., 2021; Li et al., 2015). Subsequent population explosion and long-distance migration likely facilitated high genetic exchange (Hutterer et al., 2005, Kimprasit et al., 2021, Li et al., 2015, Rodrigues & Palmeirim, 2008, Xu et al., 2005), minimizing genetic differentiation among various populations and refuges (Li et al., 2015).

Morphometric variations and taxonomic keys of three *Miniopterus* species

Our morphometric analysis reveals significant differences among three *Miniopterus* species in both body and skull size (Table 2). Specifically, *M. magnater* is slightly larger than *M. fuliginosus* and significantly larger than *M. pusillus* (Table 2). Additionally, these three species exhibited a slight male-biased SSD in skull morphology and potential geographical variation. Despite these differences, considerable morphological overlapping exists between different populations within each species, which complicates the distinguishing of morphologically similar *M. fuliginosus* and *M. magnater*. This challenge has been noted in previous studies within *Miniopterus* genus (Bilgin et al., 2012; Furman et al., 2009; Kusuminda et al., 2022; Puechmaille et al., 2014).

Hence, one of the objectives of this study was to apply a scientifically robust classification algorithm to improve classifier precision, refine the taxonomic keys, and achieve higher classification accuracy (Hothorn et al., 2006; Kotsiantis et al., 2007; Sardá-Espinosa et al., 2017). Taxonomic keys remain indispensable in modern taxonomy (Ebach & Holdrege, 2005; Zamani et al., 2022). While rapid advancements in molecular biology, particularly DNA barcoding, have gained prominence, morphological descriptions still play a vital role in biology (Ahmed et al., 2022). Our decision tree classifiers facilitate the identification of three *Miniopterus* species using FAL, BB and M^3M^3 measurements (Figure 7). *Miniopterus pusillus* is easily distinguishable by its significantly smaller body size and shorter FAL (Figure 7A, B; Kusuminda et al., 2022; Maeda, 1982). For morphologically similar species, *M. magnater* and *M. fuliginosus*, particular attention should be paid to M^3M^3 measurements (Figure 7; Kusuminda et al., 2022; Li et al., 2015; Maeda, 1982). We have also noted the limitations of traditional linear morphometrics in identifying morphologically similar species, highlighting the necessity of conducting interdisciplinary integrative analyses, such as species distribution modeling and geometric morphometric analysis, to explore potential optimal approaches for addressing these taxonomic challenges more effectively. When combined with distribution patterns identified in our study, our classifier offers

an effective tool for guiding fieldwork in *Miniopterus* species identification in China. It remains feasible to measure these variables in living individuals, thereby enhancing the accuracy of non-invasive species identification for *Miniopterus* bats.

Craniodental variations in three *Miniopterus* species

This study examined cranial size and shape variation among three *Miniopterus* species using 3D skull models. *Miniopterus pusillus* is characterized by its small body size and skull centroid size, along with such distinctive features as a narrower upturned rostrum, shorter teeth, an inflated forehead, braincase, tympanic bullae and a thinner, elongated and rounded anterior mandible (Figures 5, 6). In contrast, *M. magnater* displayed a slightly larger body size and skull centroid size, a wider and shorter rostrum, a longer palate, a deflated forehead, braincase, tympanic bullae and a well-developed and wider mandible. These traits represented subtle differences with *M. fuliginosus* (Figures 5, 6). These 3D shape variations are corroborated by linear measurements, including PL, ZB, BCH, MW, LPB, M^3M^3, ML and M_3M_3 (Table 2, ANCOVA), offering a detailed perspective on morphological changes.

Bat skull morphology has played some critical role in dietary preference (Dumont et al., 2012; Santana & Cheung, 2016; Santana et al., 2012), feeding performance (Santana & Dumont, 2009), sensory adaptations (Freeman, 1984; Pedersen, 1998; Thiagavel et al., 2018), ecological niches and evolutionary diversification (Dumont et al., 2012; Monteiro & Nogueira, 2010; Shi & Rabosky, 2015). The morphological differences existed particularly in braincase size, rostrum shape and mandibular features (Figures 5, 6). It suggested that *M. pusillus* might exhibit relatively weaker bite force, favoring a diet of smaller arthropods. In contrast, *M. magnater* possessed a stronger bite force, facilitating the consumption of hard-shelled insects (Dumont et al., 2016; Giacomini et al., 2022; Law et al., 2022). Elevated rostrum and elongated mandible of *M. pusillus*, compared to the other two species, may also indicate differences in flight pattern and echolocation capabilities (Ballell et al., 2019; Freeman, 1984; Pedersen, 1998, 2000; Wordley et al., 2014; Wu et al., 2020). These variations reinforced the adaptability of *Miniopterus* species to selective pressures, enabling them to exploit diverse ecological niches (Acero-Murcia et al., 2023; Arbour et al., 2019).

A notable finding of this study is marked variations in braincase inflation among three *Miniopterus* species. *Miniopterus pusillus* exhibited an obviously inflated braincase as compared to *M. fuliginosus* and *M. magnater* while *M. magnater* had a slightly deflated braincase relative to *M. fuliginosus* (Figures 5, 6). This variation was probably correlated with foraging and flight patterns since species foraging in open spaces often displayed smaller neocortex volume (Ratcliffe et al., 2006; Safi & Dechmann, 2005). Consequently, *M. pusillus* might prefer more complex habitats whereas *M. fuliginosus* and *M. magnater* favored open spaces (Reader & Laland, 2002; Striedter, 2005). This difference in habitat preference could help explain extensive overlapping in distribution ranges of *M. magnater* and *M. pusillus* in South China.

CONCLUSION

This study has confirmed the presence and phylogenetic relationships of three *Miniopterus* in China and highlighted their distinct ecological and morphological adaptations. *Miniopterus fuliginosus*, with its broad adaptability and extensive distribution, implied that its ancestor might have inhabited multiple Quaternary glacial refuges. In contrast, the distribution of *M. magnater* appeared to be constrained by latitude, rainfall and temperature, significantly overlapping with smaller *M. pusillus* in South China. These spatial distribution patterns provided valuable insights into their niche evolutions, highlighting the urgent necessity of proactive conservation efforts for addressing potential habitat compression. Comparative morphometric analyses, integrating traditional linear measurements and 3D geomorphometry, uncovered marked differences among three *Miniopterus* species in such traits as rostrum, forehead, tympanic bullae, braincase and mandible. These distinctions impacted divergence in ecological niches, feeding strategies and echolocation capabilities. Importantly, this study has identified, for the first time, significant variations in braincase size, correlating with differentiation in foraging and flight behaviors. Additionally, the application of decision tree classifiers effectively distinguished the taxonomic traits of three *Miniopterus* species. Key features of FAL, BB and M^3M^3 played crucial roles in species identification. In conjunctions with insights into potential distribution areas, these findings have established a robust framework for guiding future field surveys and improving the accuracy of non-invasive species identification for *Miniopterus* bats in China.

Systematics of Chinese Miniopteridae bats

Class: Mammalia

Order: Chiroptera

Family: Miniopteridae Dobson, 1857

Genus: *Miniopterus* Bonaparte, 1837

Description: *Miniopterus* bats are typical cave-dwellers, characterized by their elongated second phalanx of the third finger with nearly thrice the length of the first. Lengthened terminal part of wing folds back, creating a distinctively bent appearance. A simple muzzle lacks a nasal process or noseleaf with tail fully enclosed within uropatagium. Ears are short, triangular, rounded, partially concealed by pelage and widely separated at their bases. Head is highly domed, forming a steep forehead. Ears, muzzle, wing membranes and uropatagium are typically dark gray or dark brown to complete black. Pelage is dense and soft.

Key to species of family Miniopteridae bats from China

1a) smaller body size; FAL smaller than 43 mm, BB smaller than 7.7 mm ..... *M. pusillus*

1b) FAL larger than or equal to 43 mm, BB larger than or equal to 7.7 mm 2

2a) medium body size (a mean FAL of 48.7 mm); M^3M^3 less than 7.2 mm ..... *M. fuliginosus*

2b) larger body size (a mean FAL of 49.8 mm); M^3M^3 larger than or equal to 7.2 mm ..... *M. magnater*

Species 1: *Miniopterus magnater* Sanborn, 1931

Larger Long-fingered Bat

(Figure 8A; Table 2; Supplementary Table S5)

Type locality: Marienberg, 40 miles up Sepik River, Territory of New Guinea.

Diagnosis: Based upon our examined specimens, this is the largest-sized species among three Chinese *Miniopterus* species with a mean FAL of 49.8 mm (range 43.5–52.4 mm) and a TibL of 21.5 mm (range 20.3–23.5 mm) (Table 2). The

ears are triangular (range 8.6–14.6 mm) with slightly folded pinnae and an inward-bending outer edge of helix. Tragus is kidney-shaped, pointed at tip and slightly curved forward (Figure 8A-7). Overall fur color ranges from golden brown to saddle brown with dorsal surface darker than ventral surface (Figure 8A-7).

Skull is bulbous and slightly larger than *M. fuliginosus* in China with a mean GLS of 16.93 mm (range 16.2–17.46 mm), CBL of 16.18 mm (range 15.55–16.88 mm) and BB of 8.46 mm (range 8.09–9.62 mm) (Table 2). It also has a wider M^3M^3 and rostrum than *M. fuliginosus* (Table 2). Rostrum is flat and gently slopes to forehead with a shallow medial rostral depression (Figure 8A-1, 3). Mid-portion of braincase is lower in height than frontal region (Figure 8A-1). Well-developed sagittal crest and lambdoid crests are noted along with a well-developed zygoma and zygomata exceeding braincase in width (Figure 8A-3, 5). Hindbrain is deflated and strongly downward-deflected from mid-point of lambdoid crests (Figure 8A-1). Dental formula is I 2/3, C 1/1, P 2/3, M 3/3 (Figure 8A-6). Canines are more robust than the other two species and a noticeable gap exists between canines and incisors (Figure 8A-6). The first upper premolar (PM^2) is smaller than the second upper premolar (PM^4) and they are not in contact (Figure 8A-6). PM^4 with an additional well-developed lingual cusp posterior to main cusp, contacting the metastyle of the first upper molar (M^1) but lower than M^1 in height (Figure 8A-1, 6). M^1 and M^2 are well-developed with M^1 slightly larger than M^2 (Figure 8A-6). Palate is concave (Figure 8A-5). In mandible, pair of incisors closest to the canine is larger than the other two pairs of incisors (Figure 8A-2, 6). PM_4 is taller than PM_2 and PM_3 (Figure 8A-2). Coronoid articular processes are equal in height, with a well-developed outward-extending angular process (Figure 8A-2). Pair of infraorbital foramina and mandibular foramina are visible (Figure 8A-2). Additionally, a slightly male-biased sexual size dimorphism is noted (Supplementary Table S6).

Distribution: Yunnan, Guangxi, Guangdong, Hong Kong, Fujian and Hainan Island in China, extending across most parts of Southeast Asia (Thailand, Myanmar, Lao PDR , and Vietnam), India, Sunda Islands (Sumatra, Borneo, Java, Nusa Penida, and Timor), Central Moluccas (Seram and Ambon Islands) and New Guinea (Ibáñez & Juste, 2019; Kusuminda et al., 2022; Li et al., 2015). It may occur in Macau (refer to Discussion).

Remarks: Phylogenetic analyses revealed genetic differentiation between *M. magnater* population of Southeast Asia and New Guinea (Appleton et al., 2004; Li et al., 2015) with *ND2* gene genetic distances of ~10%. Morphological comparisons indicated that New Guinea population (type locality) was slightly larger than Chinese population (Supplementary Table S6). These findings hinted at the possibility of cryptic species within *M. magnater*. Detailed genetic studies are required for resolving the taxonomy of this group.

Species 2: *Miniopterus fuliginosus* (Hodgson, 1835)
Asian Long-fingered Bat
(Figure 8B; Table 2; Supplementary Tables S4, S6)

Type locality: Nepal.

Diagnosis: *M. fuliginosus* is medium-sized among three Chinese *Miniopterus* species with a mean FAL of 48.7 mm (range 41.3–52.2 mm) and a TibL of 20.5 mm (range 19.1–21.8 mm) (Table 2). Ears are short and triangular with a broadly rounded tip. Half of pinna is folded and ear length ranges from 8.0 to 13.7 mm (Table 2). Tragus is crescent-shaped and forwardly curved with a narrow base and a rounded tip (Figure 8B-7). Fur is deep saddle-brown to greyish-black with dorsal surface darker than ventral surface (Figure 8B-7).

Skull is bulbous and smaller than *M. magnater*, with a mean GLS of 16.30 mm (range 15.57–17.17 mm), CBL of 15.52 mm (range 14.62–16.63 mm), BB of 8.15 mm (range 7.72–8.67 mm) and M^3M^3 width of 6.93 mm (rang 6.4–7.62 mm) (Table 2). A flat rostrum gently slopes toward forehead with a shallow medial rostral depression (Figure 8B-1, 3). Sagittal

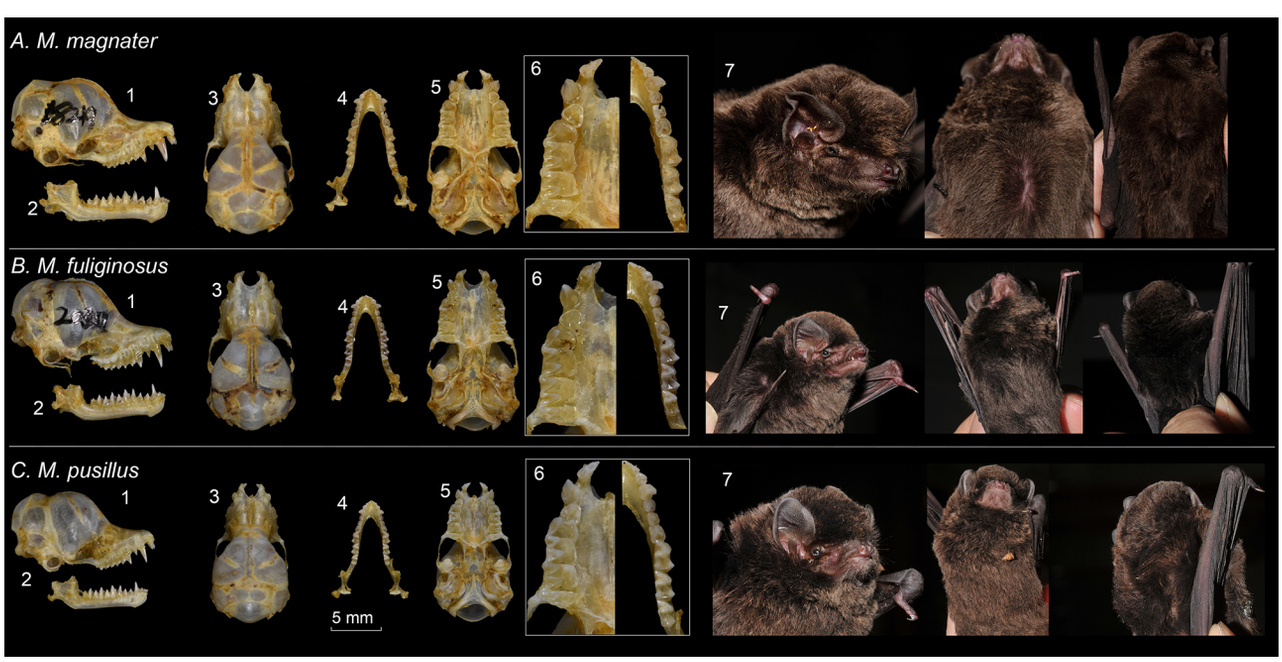

Figure 8 Skull and external features of three *Miniopterus* species from China

A. *M. magnater*; B. *M. fuliginosus*; C. *M. pusillus*; 1–2, lateral view of skull; 3–4, dorsal view of skull; 5, ventral view of skull; 6, dental surface; 7, lateral, ventral and dorsal views of external features. Photo by Yifeng Hu & Wenhua Yu.

and lambdoid crests are evident. Zygomata exceeds braincase in width (Figure 8B-3, 5). An inflated hindbrain with a smooth downward transition from mid-point of lambdoid crests (Figure 8B-1). Dental formula is I 2/3, C 1/1, P 2/3, M 3/3 (Figure 8B-6). Upper and lower canines are long and slender, with upper canines longer than lower (Figure 8B-1, 2). PM^2 is delicate and pointed, with a basal area equal to C^1, about half the height of PM^4 and not in contact with PM^4 (Figure 8B-1, 6). PM^4 has a notable lingual cusp posterior (Figure 8B-6). M^1 and M^2 are well-developed and similar in size (Figure 8B-6). Palate is concave (Figure 8B-5). Mandible is broadly rounded U-shaped (Figure 8B-4). Lower incisors are tricuspid with the pair closest to canine larger ($I_1<I_2<I_3$) (Figure 8B-2, 6). PM_4 is taller than PM_2 and PM_3 and approximately equal to M_1 in height (Figure 8B-2). Coronoid and articular processes of mandible are almost equal in height (Figure 8B-2). Pair of infraorbital foramina and mandibular foramina are evident (Figure 8B-2). Additionally, a slightly male-biased sexual size dimorphism is noted (Supplementary Table S6).

Distribution: Beijing, Hebei, Henan, Shandong, Shaanxi, Anhui, Hubei, Sichuan, Chongqing, Hunan, Jiangxi, Zhejiang, Yunnan, Guizhou, Guangxi, Guangdong, Fujian, Hong Kong, Hainan Island and Taiwan Island in China. Its range extends to Korean Peninsula, southern Russia (Far East), Japan, North India, Nepal, Myanmar, Lao PDR, Vietnam, Northeast Afghanistan and North Pakistan (Endo et al., 2019; Ibáñez & Juste, 2019; Kusuminda et al., 2022; Li et al., 2015; Thomas et al., 2013). Possible occurrences included Xinjiang and Macau (refer to Discussion) with India-Sri Lanka population requiring confirmation.

Remarks: *Miniopterus fuliginosus* was previously confused with *M. schreibersii* until current genetic and morphometric evidence confirmed it as a valid species (Appleton et al., 2004; Maeda, 1982; Tian et al., 2004). Its distribution spans a wide latitudinal range. Recent genetic studies have identified India-Sri Lanka lineage as a new species, *M. phillipsi* is slightly smaller than *M. fuliginosus* (Supplementary Table S6; Kusuminda et al., 2022). Consequently, current distribution and southern limits of *M. fuliginosus* remain unresolved. Additionally, the population of Taiwan Island exhibited slightly larger genetic distances than others (Supplementary Table S4). Future studies shall incorporate morphometric and genetic analyses for clarifying the taxonomy within this group.

Species 3: *Miniopterus pusillus* Dobson, 1876
Small Long-fingered Bats
(Figure 8C; Table 2; Supplementary Table S6)

Type locality: Nicobar (Islands, India) (Restricted by R. C. Wroughton [1918]).

Diagnosis: Based upon examined specimens, this is the smallest-sized species among three Chinese *Miniopterus* species with a mean FAL of 41.3 mm (range 39.5–43.3 mm) and a mean TibL of 17.0 mm (Table 2). Ears are small and triangular, with a mean length of 9.2 mm (range 6.0–11.9 mm) (Table 2, Figure 8C-7). The tragus is parallel-sided and minimally curved forward compared to the other two species (Figure 8C-7). Overall fur color is chocolate-brown to lighter brown (Figure 8C-7).

Skull is smaller, bulbous and delicate with a mean GLS of 14.08 mm (range 13.58–14.46 mm), a mean CBL of 13.28 mm (range 12.69–13.62 mm), a mean BB of 7.38 mm (range 7.09–7.59 mm) and a mean M^3M^3 width of 5.65 mm (range 5.36–5.89 mm) (Table 2). Rostrum is flat, short and narrow, and abruptly slopes to forehead from basal rostrum (Figure 8C-1, 3). The rostrum is slightly upturned compared to the other two species and has a shallow medial rostral depression (Figure 8C-1). The mid-portion of braincase is depressed and lower in height than frontal region. And braincase is more inflated than the other two species (Figure 8C-1). Sagittal and lambdoid crests are well-developed except in parietal region. Zygoma is slender, thinner proximally than distally, with a projection on midsection of zygoma (Figure 8C-3, 5). Zygomata is approximately equal to braincase in width (Figure 8C-3, 5). Dental formula is I 2/3, C 1/1, P 2/3, M 3/3 (Figure 8C-6). Upper canines are small and straight (Figure 8C-1). Upper incisors are visible in lateral view and a noticeable gap exists between upper incisors and upper canines (Figure 8C-1). PM^4 is well-developed and larger than PM^2, and they are not in contact (Figure 8C-6). M^1 and M^2 are well-developed with M^1 slightly larger (Figure 8C-6). Palate is concave (Figure 8C-5). I_3 is larger than the other lower incisors (Figure 8C-6). PM_2 to PM_4 progressively increases in size, with PM_4 having an additional well-developed lingual cusp posterior to main cusp (Figure 8C-6). PM_4 is approximately equal to M_1 and M_2 in height (Figure 8C-2). M_1 is slightly larger than M_2 and both are significantly larger than M_3 in size (Figure 8C-6). Mandible is delicate with smooth mandibular gnathion (Figure 8C-2, 4).

Distribution: Yunnan, Guangxi, Guangdong, Hong Kong, Macau, Fujian and Hainan Island in China. Its residing range extends to Nepal, North India, Southeast Asia (Thailand, Myanmar, Lao PDR, Vietnam & Cambodia) and part of insular Southeast Asia (Nicobar Island, Sumatra, Java, Sulawesi, Lesser Sundas & Moluccas) (Ibáñez & Juste, 2019; Srinivasulu & Srinivasulu, 2023). Borneo requires confirmation.

Remarks: *Miniopterus pusillus* is a small-sized long-fingered bat with limited prior studies. Current phylogenetic and morphological analyses have uncovered a cryptic species, *M. srinii* (slighter smaller than *M. pusillus*, Supplementary Table S6), from South India, previously misidentified as "*M. pusillus*" (Srinivasulu & Srinivasulu, 2023). However, unresolved phylogenetic relationships remain between populations from Nicobar Islands (type locality) and other South Asia, Southeast Asia and Northeast India regions. Our Chinese specimens were notably larger than those of Nicobar Islands (Supplementary Table S6). Future studies of genetic and morphometric analyses are essential for resolving these systematic uncertainties.

SCIENTIFIC FIELD SURVEY PERMISSION INFORMATION

Sample collections in the field were conducted following the Wildlife Protection Law of the People's Republic of China.

DATA AVAILABILITY

The newly generated cytochrome c oxidase subunit 1 (*COI*) sequences, and the R scripts for 3D skull geometric morphometrics, species distribution modeling and decision tree classifier analyses of this study are accessible on Science Data Bank (http://www.scidb.cn/) under DOI: 10.57760/sciencedb.zrdc.00017.

SUPPLEMENTARY DATA

Supplementary data to this article can be found online.

COMPETING INTERESTS

The authors declare that they have no competing interests.

AUTHORS' CONTRIBUTIONS

Y.F.H., X.Y.W., Y.W., M.M. and W.H.Y. designed and supervised this study. Y.F.H. processed the samples and performed molecular assays, phylogenetic analysis, 3D skull modeling, geomorphometry, species distribution modeling and statistical analyses. Y.F.H. and X.Y.W. composed manuscript. All authors revised manuscript. All authors read and approved the final version of the manuscript.

REFERENCES

Acero-Murcia AC, Severgnini MR, Fischer E, et al. 2023. An evolutionary ecomorphological perspective on the assembly of a Neotropical bat metacommunity. *Journal of Mammalian Evolution*, **30**(3): 627–640.

Adams DC, Collyer M, Kaliontzopoulou A, et al. 2022. Geomorph: software for geometric morphometric analyses. R package. https://CRAN.R-project.org/package=geomorph.

Adler D, Murdoch D. 2020. Package rgl. R package. https://CRAN.R-project.org/package=rgl.

Ahmed S, Ibrahim M, Nantasenamat C, et al. 2022. Pragmatic applications and universality of DNA barcoding for substantial organisms at species level: a review to explore a way forward. *BioMed Research International*, **2022**: 1846485.

Alhajeri BH. 2021. Cranial variation in allactagine jerboas (Allactaginae, Dipodidae, Rodentia): a geometric morphometric study. *Zoological Research*, **42**(2): 182–194.

Amengual B, López-Roig M, Serra-Cobo J. 2007. First record of seasonal over sea migration of *Miniopterus schreibersii* and *Myotis capaccinii* between Balearic Islands (Spain). *Acta Chiropterologica*, **9**(1): 319–322.

Ancillotto L, Fichera G, Pidinchedda E, et al. 2021. Wildfires, heatwaves and human disturbance threaten insular endemic bats. *Biodiversity and Conservation*, **30**(14): 4401–4416.

Appleton BR, Mckenzie JA, Christidis L. 2004. Molecular systematics and biogeography of the bent-wing bat complex *Miniopterus schreibersii* (Kuhl, 1817) (Chiroptera: Vespertilionidae). *Molecular Phylogenetics and Evolution*, **31**(2): 431–439.

Araújo MB, New M. 2007. Ensemble forecasting of species distributions. *Trends in Ecology & Evolution*, **22**(1): 42–47.

Arbour JH, Curtis AA, Santana SE. 2019. Signatures of echolocation and dietary ecology in the adaptive evolution of skull shape in bats. *Nature Communications*, **10**(1): 2036.

Arthur L, Lemaire M, Dufrêne L, et al. 2014. Understanding bat-habitat associations and the effects of monitoring on long-term roost success using a volunteer dataset. *Acta Chiropterologica*, **16**(2): 397–411.

Ballell A, Moon BC, Porro LB, et al. 2019. Convergence and functional evolution of longirostry in crocodylomorphs. *Palaeontology*, **62**(6): 867–887.

Bilgin R, Gürün K, Maraci Ö, et al. 2012. Syntopic occurrence in Turkey supports separate species status for *Miniopterus schreibersii schreibersii* and *M. schreibersii pallidus* (Mammalia: Chiroptera). *Acta Chiropterologica*, **14**(2): 279–289.

Bodenhofer U, Bonatesta E, Horejš-Kainrath C, et al. 2015. msa: an R package for multiple sequence alignment. *Bioinformatics*, **31**(24): 3997–3999.

Bosso L, Ancillotto L, Smeraldo S, et al. 2018. Loss of potential bat habitat following a severe wildfire: a model-based rapid assessment. *International Journal of Wildland Fire*, **27**(11): 756–769.

Bronrier GN, Maloney SK, Buffenstein R. 1999. Survival tactics within thermally-challenging roosts: heat tolerance and cold sensitivity in the Angolan free-tailed bat. *Mops condylurus*. *South African Journal of Zoology*, **34**(1): 1–10.

Brown DE, Corruble V, Pittard CL. 1993. A comparison of decision tree classifiers with backpropagation neural networks for multimodal classification problems. *Pattern Recognition*, **26**(6): 953–961.

Burke RA, Frey JK, Ganguli A, et al. 2019. Species distribution modelling supports "nectar corridor" hypothesis for migratory nectarivorous bats and conservation of tropical dry forest. *Diversity and Distributions*, **25**(9): 1399–1415.

Cao WZ, Mirjalili V, Raschka S. 2020. Rank consistent ordinal regression for neural networks with application to age estimation. *Pattern Recognition Letters*, **140**: 325–331.

Chi Y, Wang JC, Xi CB, et al. 2020. Spatial pattern of species richness among terrestrial mammals in China. *Diversity*, **12**(3): 96.

Das TK. 2015. A customer classification prediction model based on machine learning techniques. *In*: Proceedings of 2015 International Conference on Applied and Theoretical Computing and Communication Technology. Davangere: IEEE, 321–326.

De'ath G, Fabricius KE. 2000. Classification and regression trees: a powerful yet simple technique for ecological data analysis. *Ecology*, **81**(11): 3178–3192.

Delgado-Jaramillo M, Aguiar LMS, Machado RB, et al. 2020. Assessing the distribution of a species-rich group in a continental-sized megadiverse country: bats in Brazil. *Diversity and Distributions*, **26**(5): 632–643.

Dong PP, Gao WJ, Wang RR, et al. 2023. Local bats diversity exceeded the regional bats diversity in Xinjiang, China. *Authorea*, doi: 10.22541/au.168374638.84859976/v1.

Dumont ER, Dávalos LM, Goldberg A, et al. 2012. Morphological innovation, diversification and invasion of a new adaptive zone. *Proceedings of the Royal Society B: Biological Sciences*, **279**(1734): 1797–1805.

Dumont M, Wall CE, Botton-Divet L, et al. 2016. Do functional demands associated with locomotor habitat, diet, and activity pattern drive skull shape evolution in musteloid carnivorans?. *Biological Journal of the Linnean Society*, **117**(4): 858–878.

Ebach MC, Holdrege C. 2005. DNA barcoding is no substitute for taxonomy. *Nature*, **434**(7034): 697.

Endo K, Iida K, Nunome M, et al. 2019. Phylogeography of *Miniopterus fuliginosus* (Chiroptera) with special reference to Jeju Island, South Korea. *Mammalia*, **83**(6): 610–614.

Fedorov A, Beichel R, Kalpathy-Cramer J, et al. 2012. 3D Slicer as an image computing platform for the Quantitative Imaging Network. *Magnetic Resonance Imaging*, **30**(9): 1323–1341.

Festa F, Ancillotto L, Santini L, et al. 2023. Bat responses to climate change: a systematic review. *Biological Reviews*, **98**(1): 19–33.

Fick SE, Hijmans RJ. 2017. WorldClim 2: new 1-km spatial resolution climate surfaces for global land areas. *International Journal of Climatology*, **37**(12): 4302–4315.

Francis CM, Borisenko AV, Ivanova NV, et al. 2010. The role of DNA barcodes in understanding and conservation of mammal diversity in Southeast Asia. *PLoS One*, **5**(9): e12575.

Freeman PW. 1984. Functional cranial analysis of large animalivorous bats (Microchiroptera). *Biological Journal of the Linnean Society*, **21**(4): 387–408.

Friedman JH, Popescu BE. 2008. Predictive learning via rule ensembles. *The Annals of Applied Statistics*, **2**(3): 916–954.

Fu JZ, Wen LY. 2023. Impacts of Quaternary glaciation, geological history and geography on animal species history in continental East Asia: a phylogeographic review. *Molecular Ecology*, **32**(16): 4497–4514.

Furman A, Çoraman E, Bilgin R, et al. 2009. Molecular ecology and phylogeography of the bent-wing bat complex (*Miniopterus schreibersii*) (Chiroptera: Vespertilionidae) in Asia Minor and adjacent regions. *Zoologica Scripta*, **38**(2): 129–141.

Furman A, Postawa T, Öztunç T, et al. 2010. Cryptic diversity of the bent-wing bat, *Miniopterus schreibersii* (Chiroptera: Vespertilionidae), in Asia Minor. *BMC Evolutionary Biology*, **10**: 121.

Gao S, Calhoun VD, Sui J. 2018. Machine learning in major depression: from classification to treatment outcome prediction. *CNS Neuroscience & Therapeutics*, **24**(11): 1037–1052.

Giacomini G, Herrel A, Chaverri G, et al. 2022. Functional correlates of skull shape in Chiroptera: feeding and echolocation adaptations. *Integrative Zoology*, **17**(3): 430–442.

Goodman SM, Ramasindrazana B, Naughton KM, et al. 2015. Description of a new species of the *Miniopterus aelleni* group (Chiroptera: Miniopteridae) from upland areas of central and northern Madagascar. *Zootaxa*, **3936**(4): 538–558.
Grenouillet G, Buisson L, Casajus N, et al. 2011. Ensemble modelling of species distribution: the effects of geographical and environmental ranges. *Ecography*, **34**(1): 9–17.
Guisan A, Thuiller W. 2005. Predicting species distribution: offering more than simple habitat models. *Ecology Letters*, **8**(9): 993–1009.
Hao TX, Elith J, Lahoz-Monfort JJ, et al. 2020. Testing whether ensemble modelling is advantageous for maximising predictive performance of species distribution models. *Ecography*, **43**(4): 549–558.
Hardy SM, Lindgren M, Konakanchi H, et al. 2011. Predicting the distribution and ecological niche of unexploited snow crab (*Chionoecetes opilio*) populations in Alaskan waters: a first open-access ensemble model. *Integrative and Comparative Biology*, **51**(4): 608–622.
He K, Jiang XL. 2014. Sky islands of Southwest China. I: an overview of phylogeographic patterns. *Chinese Science Bulletin*, **59**(7): 585–597.
Hijmans RJ, Van Etten J, Cheng J, et al. 2015. Package 'raster'. R package. https://CRAN.R-project.org/package=raster.
Hoang DT, Chernomor O, von Haeseler A, et al. 2018. UFBoot2: improving the ultrafast bootstrap approximation. *Molecular Biology and Evolution*, **35**(2): 518–522.
Hothorn T, Hornik K, Zeileis A. 2006. Unbiased recursive partitioning: a conditional inference framework. *Journal of Computational and Graphical Statistics*, **15**(3): 651–674.
Hutterer R, Ivanova T, Meyer-Cords C, et al. 2005. Bat Migrations in Europe: a Review of Banding Data and Literature. Münster: BfN-Schriftenvertrieb im Landwirtschaftsverlag.
Ibáñez C, Juste J. 2019. Family Miniopteridae (long-fingered bats). *In*: Wilson DE, Mittermeier RA. Handbook of the Mammals of the World: Vol. 9: Bats. Barcelona: Lynx Ediciones, 674–709.
Ke C, Gong LX, Geng Y, et al. 2024. Patterns and correlates of potential range shifts of bat species in China in the context of climate change. *Conservation Biology*, **6**: e14310.
Kimprasit T, Nunome M, Iida K, et al. 2021. Dispersal history of *Miniopterus fuliginosus* bats and their associated viruses in East Asia. *PLoS One*, **16**(1): e0244006.
Kotsiantis SB, Zaharakis I, Pintelas P. 2007. Supervised machine learning: a review of classification techniques. *Emerging Artificial Intelligence Applications in Computer Engineering*, **160**(1): 3–24.
Kusuminda T, Mannakkara A, Ukuwela KDB, et al. 2022. DNA barcoding and morphological analyses reveal a cryptic species of *Miniopterus* from India and Sri Lanka. *Acta Chiropterologica*, **24**(1): 1–17.
Law CJ, Blackwell EA, Curtis AA, et al. 2022. Decoupled evolution of the cranium and mandible in carnivoran mammals. *Evolution*, **76**(12): 2959–2974.
Li S, Sun KP, Lu GJ, et al. 2015. Mitochondrial genetic differentiation and morphological difference of *Miniopterus fuliginosus* and *Miniopterus magnater* in China and Vietnam. *Ecology and Evolution*, **5**(6): 1214–1223.
Liang J, Yang XL, Li B, et al. 2017. Detection of diverse viruses in alimentary specimens of bats in Macau. *Virologica Sinica*, **32**(3): 226–234.
Lisón F, Espín S, Aroca B, et al. 2017. Assessment of mercury exposure and maternal-foetal transfer in *Miniopterus schreibersii* (Chiroptera: Miniopteridae) from southeastern Iberian Peninsula. *Environmental Science and Pollution Research*, **24**(6): 5497–5508.
Maeda K. 1982. Studies on the classification of *Miniopterus* in Eurasia, Australia and Melanesia. *Honyurui Kagaku* (*Mammalian Science*), **Supplement. 1**: 1–176.
Maniruzzaman M, Rahman MJ, Ahammed B, et al. 2020. Classification and prediction of diabetes disease using machine learning paradigm. *Health Information Science and Systems*, **8**(1): 7.
Măntoiu DŞ, Mirea IC, Şandric IC, et al. 2022. Bat dynamics modelling as a tool for conservation management in subterranean environments. *PLoS One*, **17**(10): e0275984.
Marcus LF, Corti M, Loy A, et al. 2013. Advances in Morphometrics. New York: Springer.
Merow C, Smith MJ, Silander Jr JA. 2013. A practical guide to MaxEnt for modeling species' distributions: what it does, and why inputs and settings matter. *Ecography*, **36**(10): 1058–1069.
Messner E, Fediuk M, Swatek P, et al. 2020. Multi-channel lung sound classification with convolutional recurrent neural networks. *Computers in Biology and Medicine*, **122**: 103831.
Monadjem A, Guyton J, Naskrecki P, et al. 2020. Cryptic diversity in the genus *Miniopterus* with the description of a new species from southern Africa. *Acta Chiropterologica*, **22**(1): 1–19.
Monadjem A, Shapiro JT, Richards LR, et al. 2019. Systematics of West African *Miniopterus* with the description of a new species. *Acta Chiropterologica*, **21**(2): 237–256.
Monteiro LR, Nogueira MR. 2010. Adaptive radiations, ecological specialization, and the evolutionary integration of complex morphological structures. *Evolution*, **64**(3): 724–744.
Mou X, Qian YS, Li M, et al. 2024. A new species of *Murina* (Chiroptera: Vespertilionidae) from Yunnan, China. *Animals*, **14**(16): 2371.
Naimi B, Araújo MB. 2016. sdm: a reproducible and extensible R platform for species distribution modelling. *Ecography*, **39**(4): 368–375.
Naimi B, Hamm NAS, Groen TA, et al. 2014. Where is positional uncertainty a problem for species distribution modelling?. *Ecography*, **37**(2): 191–203.
Nguyen LT, Schmidt HA, Von Haeseler A, et al. 2015. IQ-TREE: a fast and effective stochastic algorithm for estimating maximum-likelihood phylogenies. *Molecular Biology and Evolution*, **32**(1): 268–274.
Novella-Fernandez R, Juste J, Ibáñez C, et al. 2021. Broad-scale patterns of geographic avoidance between species emerge in the absence of fine-scale mechanisms of coexistence. *Diversity and Distributions*, **27**(9): 1606–1618.
Oeser J, Zurell D, Mayer F, et al. 2024. The best of two worlds: using stacked generalisation for integrating expert range maps in species distribution models. *Global Ecology and Biogeography*, **33**(12): e13911.
Paluh DJ, Bauer AM. 2017. Comparative skull anatomy of terrestrial and crevice-dwelling *Trachylepis skinks* (Squamata: Scincidae) with a survey of resources in scincid cranial osteology. *PLoS One*, **12**(9): e0184414.
Pedersen SC. 1998. Morphometric analysis of the chiropteran skull with regard to mode of echolocation. *Journal of Mammalogy*, **79**(1): 91–103.
Pedersen SC. 2000. Skull growth and the acoustical axis of the head in bats. *In*: Adams RA, Pedersen SC. Ontogeny, Functional Ecology, and Evolution of Bats. Cambridge: Cambridge University Press, 174–213.
Porto A, Rolfe S, Maga AM. 2021. ALPACA: a fast and accurate computer vision approach for automated landmarking of three-dimensional biological structures. *Methods in Ecology and Evolution*, **12**(11): 2129–2144.
Puechmaille SJ, Allegrini B, Benda P, et al. 2014. A new species of the *Miniopterus schreibersii* species complex (Chiroptera: Miniopteridae) from the Maghreb region, North Africa. *Zootaxa*, **3794**(1): 108–124.
Rahbek C, Borregaard MK, Antonelli A, et al. 2019. Building mountain biodiversity: geological and evolutionary processes. *Science*, **365**(6458): 1114–1119.
Ratcliffe JM, Fenton MB, Shettleworth SJ. 2006. Behavioral flexibility positively correlated with relative brain volume in predatory bats. *Brain, Behavior and Evolution*, **67**(3): 165–176.
Reader SM, Laland KN. 2002. Social intelligence, innovation, and enhanced brain size in primates. *Proceedings of the National Academy of Sciences of the United States of America*, **99**(7): 4436–4441.
Rebelo H, Tarroso P, Jones G. 2010. Predicted impact of climate change on European bats in relation to their biogeographic patterns. *Global Change Biology*, **16**(2): 561–576.
Rodrigues L, Palmeirim JM. 2008. Migratory behaviour of the Schreiber's bat: when, where and why do cave bats migrate in a Mediterranean region?. *Journal of Zoology*, **274**(2): 116–125.
Rohlf FJ, Slice D. 1990. Extensions of the Procrustes method for the

optimal superimposition of landmarks. *Systematic Biology*, **39**(1): 40–59.
Ronquist F, Teslenko M, van der Mark P, et al. 2012. MrBayes 3.2: efficient Bayesian phylogenetic inference and model choice across a large model space. *Systematic Biology*, **61**(3): 539–542.
Safi K, Dechmann DKN. 2005. Adaptation of brain regions to habitat complexity: a comparative analysis in bats (Chiroptera). *Proceedings of the Royal Society B: Biological Sciences*, **272**(1559): 179–186.
Salinas-Ramos VB, Ancillotto L, Cistrone L, et al. 2021. Artificial illumination influences niche segregation in bats. *Environmental Pollution*, **284**: 117187.
Sanborn CC. 1931. Bats from Polynesia, Melanesia, and Malaysia. Chicago: Field Museum of Natural History, 17.
Santana SE, Cheung E. 2016. Go big or go fish: morphological specializations in carnivorous bats. *Proceedings of the Royal Society B: Biological Sciences*, **283**(1830): 20160615.
Santana SE, Dumont ER. 2009. Connecting behaviour and performance: the evolution of biting behaviour and bite performance in bats. *Journal of Evolutionary Biology*, **22**(11): 2131–2145.
Santana SE, Grosse IR, Dumont ER. 2012. Dietary hardness, loading behavior, and the evolution of skull form in bats. *Evolution*, **66**(8): 2587–2598.
Sardá-Espinosa A, Subbiah S, Bartz-Beielstein T. 2017. Conditional inference trees for knowledge extraction from motor health condition data. *Engineering Applications of Artificial Intelligence*, **62**: 26–37.
Scherrer D, Christe P, Guisan A. 2019. Modelling bat distributions and diversity in a mountain landscape using focal predictors in ensemble of small models. *Diversity and Distributions*, **25**(5): 770–782.
Schlager S. 2017. Morpho and Rvcg-shape analysis in R: R-packages for geometric morphometrics, shape analysis and surface manipulations. *In*: Zheng GY, Li S, Székely G. Statistical shape and deformation analysis. London: Academic Press, 217–256.
Schmitt S, Pouteau R, Justeau D, et al. 2017. SSDM: an R package to predict distribution of species richness and endemism based on stacked species distribution models. *Methods in Ecology and Evolution*, **8**(12): 1795–1803.
Sen PC, Hajra M, Ghosh M. 2020. Supervised classification algorithms in machine learning: a survey and review. *In*: Mandal JK, Bhattacharya D. Emerging Technology in Modelling and Graphics: Proceedings of IEM Graph 2018. Singapore: Springer, 99–111.
Shi JJ, Rabosky DL. 2015. Speciation dynamics during the global radiation of extant bats. *Evolution*, **69**(6): 1528–1545.
Simmons NB. 2005. Subfamily Miniopterinae. *In*: Wilson DE, Reeder DM. Mammal Species of the World: A Taxonomic and Geographic Reference. 3rd ed. Baltimore: Johns Hopkins University Press, 519–521.
Smeraldo S, Bosso L, Salinas-Ramos VB, et al. 2021. Generalists yet different: distributional responses to climate change may vary in opportunistic bat species sharing similar ecological traits. *Mammal Review*, **51**(4): 571–584.
Smeraldo S, Di Febbraro M, Bosso L, et al. 2018. Ignoring seasonal changes in the ecological niche of non-migratory species may lead to biases in potential distribution models: lessons from bats. *Biodiversity and Conservation*, **27**(9): 2425–2441.
Smith AT, Xie Y. 2008. A Guide to the Mammals of China. Princeton: Princeton University Press, 380–382.
Srinivasulu A, Zeale MRK, Srinivasulu B, et al. 2024. Future climatically suitable areas for bats in South Asia. *Ecology and Evolution*, **14**(5): e11420.
Srinivasulu B, Srinivasulu A. 2023. A new species of the *Miniopterus australis* species complex (Chiroptera: Miniopteridae) from the Western Ghats, India. *Zootaxa*, **5296**(2): 233–249.
Striedter GF. 2005. Principles of Brain Evolution. Sunderland: Sinauer Associates.
Su HX, Wang YY, Han YL, et al. 2023. Discovery and characterization of novel paramyxoviruses from bat samples in China. *Virologica Sinica*, **38**(2): 198–207.
Sun XY, Huang N, Zhou WW. 2022. Geographical patterns in functional diversity of Chinese terrestrial vertebrates. *Diversity*, **14**(11): 987.
Tamura K, Stecher G, Kumar S. 2021. MEGA11: molecular evolutionary genetics analysis version 11. *Molecular Biology and Evolution*, **38**(7): 3022–3027.
The R Foundation. 2023. The R project for statistical computing. http://www.R-project.org/.
Therneau T, Atkinson B, Ripley B. 2015. rpart: recursive partitioning and regression trees. R package. https://CRAN.R-project.org/package=rpart.
Thiagavel J, Cechetto C, Santana SE, et al. 2018. Auditory opportunity and visual constraint enabled the evolution of echolocation in bats. *Nature Communications*, **9**(1): 98.
Thomas NM, Duckworth JW, Douangboubpha B, et al. 2013. A checklist of bats (Mammalia: Chiroptera) from Lao PDR. *Acta Chiropterologica*, **15**(1): 193–260.
Thompson JD, Higgins DG, Gibson TJ. 1994. CLUSTAL W: improving the sensitivity of progressive multiple sequence alignment through sequence weighting, position-specific gap penalties and weight matrix choice. *Nucleic Acids Research*, **22**(22): 4673–4680.
Tian LX, Liang B, Maeda K, et al. 2004. Molecular studies on the classification of *Miniopterus schreibersii* (Chiroptera: Vespertilionidae) inferred from mitochondrial cytochrome *b* sequences. *Folia Zoologica*, **53**(3): 303–311.
Wan A, Dunlap L, Ho D, et al. 2020. NBDT: neural-backed decision trees. *arXiv*, doi: https://doi.org/10.48550/arXiv.2004.00221.
Wang R, Li ZM, Peng QM, et al. 2023. High prevalence and genetic diversity of hemoplasmas in bats and bat ectoparasites from China. *One Health*, **16**: 100498.
Wang YX. 2003. A Complete Checklist of Mammal Species and Subspecies in China: a Taxonomic and Geographic Reference. Beijing: China Forestry Publishing House. (in Chinese)
Webb PI, Speakman JR, Racey PA. 1996. How hot is a hibernaculum? A review of the temperatures at which bats hibernate. *Canadian Journal of Zoology*, **74**(4): 761–765.
Wieringa JG, Carstens BC, Gibbs HL. 2021. Predicting migration routes for three species of migratory bats using species distribution models. *PeerJ*, **9**: e11177.
Wordley CFR, Foui EK, Mudappa D, et al. 2014. Acoustic identification of bats in the southern Western Ghats, India. *Acta Chiropterologica*, **16**(1): 213–222.
Wu H, Jiang TL, Liu S, et al. 2020. Acoustic identification of two morphologically similar bat species, *Miniopterus magnater* and *Miniopterus fuliginosus* (Chiroptera, Miniopteridae). *Mammalia*, **84**(2): 201–206.
Xu H, Maeda K, Inoue R, et al. 2005. Migration of young bent-winged bats, *Miniopterus fuliginosus* born in Shirahama, Wakayama Prefecture (1) Records from the years 2003 and 2004. *Bulletin of Center for Natural Environment Education, Nara University of Education*, **7**: 31-37 (in Japanese).
Zamani A, Dal Pos D, Fric ZF, et al. 2022. The future of zoological taxonomy is integrative, not minimalist. *Systematics and Biodiversity*, **20**(1): 1–14.
Zelditch M, Swiderski DL, Sheets HD. 2012. Geometric Morphometrics for Biologists: A Primer. 2nd ed. Amsterdam: Academic Press.
Zhang CM, Jiang TL, Lu GJ, et al. 2018. Geographical variation in the echolocation calls of bent-winged bats. *Miniopterus fuliginosus. Zoology*, **131**: 36–44.
Zhang DR, Hui H, Yu GH, et al. 2020. Shared response to changes in drainage basin: phylogeography of the Yunnan small narrow-mouthed frog, *Glyphoglossus yunnanensis* (Anura: Microhylidae). *Ecology and Evolution*, **10**(3): 1567–1580.